

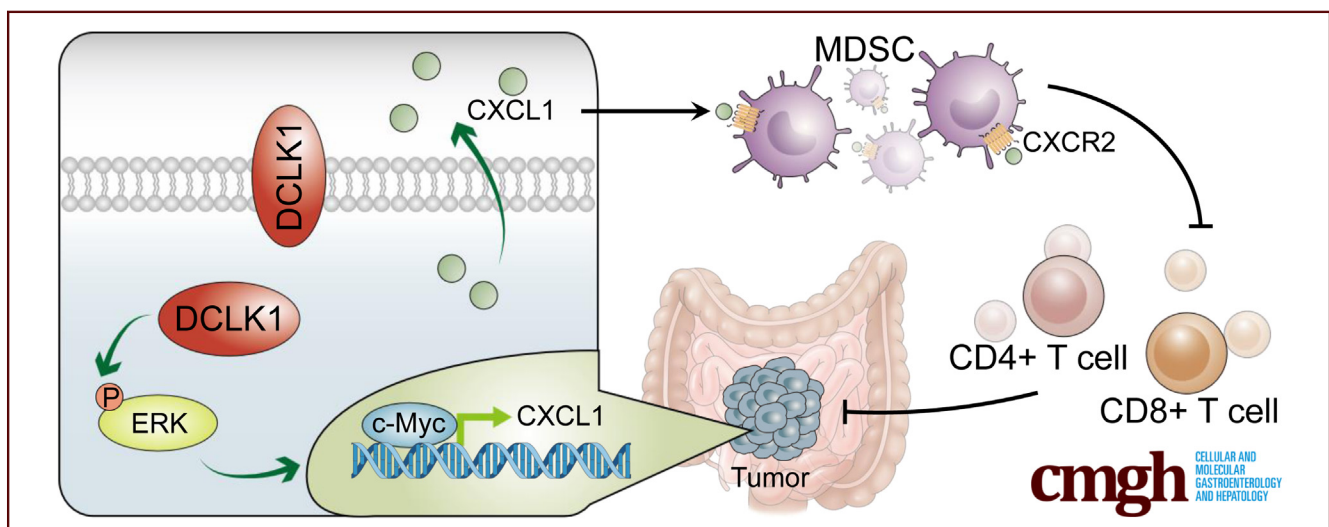
ORIGINAL RESEARCH

DCLK1 Suppresses Tumor-Specific Cytotoxic T Lymphocyte Function Through Recruitment of MDSCs via the CXCL1-CXCR2 Axis



Rui Yan,^{1,*} Jianjian Li,^{2,*} Zeru Xiao,¹ Xiaona Fan,¹ Heshu Liu,¹ Ying Xu,² Ruya Sun,² Jian Liu,¹ Jiannan Yao,¹ Guangyu An,¹ Yan Shi,^{2,3} and Yang Ge¹

¹Beijing Chao-Yang Hospital, Department of Oncology, Capital Medical University, Beijing, China; ²Institute for Immunology, Department of Basic Medical Sciences, School of Medicine, Tsinghua-Peking Center for Life Sciences, Tsinghua University, Beijing, China; and ³Institute for Immunology, Beijing Key Lab for Immunological Research on Chronic Diseases, School of Medicine, Tsinghua University, Beijing, China



SUMMARY

High expression of doublecortin-like kinase 1 (DCLK1) in intestinal cancer suggests a poor prognosis. DCLK1 promotes tumor immune evasion through C-X-C motif ligand 1-mediated myeloid-derived suppressor cell recruitment. Abolishing myeloid-derived suppressor cell infiltration by chemokine C-X-C motif receptor 2 blockade eliminates the immune privilege of DCLK1+ tumor and leads to tumor regression.

BACKGROUND & AIMS: Gastrointestinal cancer stem cell marker doublecortin-like kinase (DCLK1) is strongly associated with poor outcomes in colorectal cancer (CRC). Although DCLK1's regulatory effect on the tumor immune microenvironment has been hypothesized, its mode of action has not been shown previously *in vivo*, which hampers the potential intervention based on this molecule for clinical practice.

METHODS: To define the immunomodulatory mechanisms of DCLK1 *in vivo*, we generated DCLK1^{-/-} tumor cells by Clustered regularly interspaced short palindromic repeats (CRISPR)-

CRISPR-associated protein 9 (Cas9) and developed subcutaneous and intestinal orthotopic transplantation tumor models. Tumor tissues were harvested and subjected to immunofluorescence staining, flow cytometry analysis of tumor-infiltrating immune cell populations, tumor myeloid-derived suppressor cell (MDSC) sorting by isolation kit and then co-culture with spleen T cells, and RNA sequencing for transcriptomic analysis.

RESULTS: We found that DCLK1^{-/-} tumor cells lose their tumorigenicity under immune surveillance. Failed tumor establishment of DCLK1^{-/-} was associated with an increase in infiltration of CD8⁺ T cells and effector CD4⁺ T cells, and reduced numbers of MDSCs in the tumor tissue. Furthermore, DCLK1 promoted the up-regulation of C-X-C motif ligand 1, which recruits MDSCs in CRC through chemokine C-X-C motif receptor 2. The ability of *in vivo* tumor growth of DCLK1^{-/-} tumor cells was rescued by C-X-C motif ligand 1 over-expression. Collectively, we validated that DCLK1 promotes tumor growth in CRC through recruitment of T-cell-suppressive MDSCs.

CONCLUSIONS: DCLK1-mediated immune suppression in tumor models allows escaping from the host's antitumor response. Because DCLK1 is one of the most common markers in gastrointestinal tumors, these results identify a precise

therapeutic target for related clinical interventions. (*Cell Mol Gastroenterol Hepatol* 2023;15:463–485; <https://doi.org/10.1016/j.jcmgh.2022.10.013>)

Keywords: DCLK1; Colorectal Carcinoma; Tumor Microenvironment; Immune Escape; MDSCs.

Colorectal cancer (CRC) is the most common malignancy in the digestive system and the third leading cause of cancer mortality.¹ Although colonoscopy is widely used, many patients diagnosed with CRC during the first visit are already in the advanced stage. Because of limitations of traditional chemotherapy and radiotherapy, more than 50% of patients die from CRC recurrence and metastasis.^{1,2} Immunotherapy, particularly immune checkpoint blockade, is proven to be effective against non-small-cell lung cancer, renal carcinoma, and melanoma. However, immune checkpoint therapy has a limited 5% success rate in advanced CRC patients and is only effective in those with the uncommon microsatellite instability-high subtype, which responds well to programmed cell death protein-1/programmed cell death-ligand 1 inhibitors. For the majority of CRC patients afflicted with microsatellite stable (MSS) tumors, immunotherapy is largely ineffective.^{3,4} Therefore, it is necessary to explore new targets for CRC immunotherapy.

Cancer stem cells (CSCs) are a group of cells with self-renewal and multi-differentiation potential. The occurrence and development of tumors are closely related to CSCs, and CRC is no exception.⁵ Residing in various anatomic and immunologic niches, CSCs form a unique tumor microenvironment (TME) with stromal cells and immune cells.^{6–8} In the TME, CSCs promote the invasion and metastasis of tumor cells via several mechanisms, including enhanced angiogenesis and cytokine production.⁹ In addition, immunosuppressive cells like tumor-associated macrophages (TAMs), regulatory T cells (Tregs), and myelosuppressive cells infiltrating in the TME inhibit the cytolytic function of CD8⁺ T cells and natural killer (NK) cells by secreting transforming growth factor- β (TGF- β), IL6, and other cytokines.^{6,9} This process is widely regarded as highly conducive to tumor immune escape, and disrupting immunosuppressive TME through targeting CSCs is emerging as a potential precision target in the treatment of CRC.

In gastrointestinal cancer, doublecortin-like kinase 1 (DCLK1) is a CSC biomarker related to tumor development.^{10,11} High expression of DCLK1 is found in both human and mouse CRC tissues.^{12–14} DCLK1-positive cells in CRC have increased invasive and metastatic capacity, with a corresponding high antigen Ki-67 proliferation index and anti-apoptotic protein expression.¹⁵ In an *APC^{Min/+}* mouse-derived spontaneous tumor model, deletion of the DCLK1 marked tumor stem cell resulted in the regression of polyps.¹³ Importantly, previous studies have shown that the high expression of DCLK1 in gastrointestinal tumors is associated significantly with a poor prognosis.^{16,17}


Although DCLK1 is an ideal biomarker of gastrointestinal CSCs, its role in the tumor immune

microenvironment only recently has been noticed. The study by Zhang et al¹⁸ in 2018 showed the relationship between DCLK1 and tumor immune microenvironment in the pancreatic cancer mouse model. Through gene expression profiling, they discovered that IL17 secreted by immune cells could stimulate the expression of certain CSC molecules, such as aldehyde-dehydrogenase 1A1 and, interestingly, DCLK1. This stimulation eventually led to the development of an initial lesion of the pancreatic duct and the establishment of adenocarcinoma. Another study showed that in the Villin^{Cre}; *Dclk1^{flox/flox}* model, mice with this DCLK1 deficiency suffered a more severe degree of inflammatory bowel disease with immune factors varying significantly from the controls, such as IL17, IL1 β , CXCL1, and CXCL2.¹⁹ These findings suggest that DCLK1 may play an important role in the regulation of immune response. Recently, Sureban et al²⁰ designed a DCLK1-related chimeric antigen-receptor T-cell immunotherapy for CRC. This chimeric antigen-receptor T-cell therapy can inhibit the proliferation of CRC cells both *in vivo* and *in vitro*, without any severe side effects. However, the underlying mechanism of DCLK1 giving rise to this potential clinical implication has yet to be shown.

To further study how DCLK1 regulates host immunity, a high priority should be given to whether this molecule regulates TME *in vivo*. Increasing evidence indicates that tumor immune evasion involves many immunosuppressive cells in the TME. Among them, myeloid-derived suppressor cells (MDSCs), which first were identified in 2007, are under intensive scrutiny. At the moment, studies on MDSCs mainly focus on their immunosuppressive function in the process of tumor initiation.^{21–23} Originating from myeloid tissues, MDSCs are immature cells derived from myeloid precursor cells. MDSCs are characterized by myeloid cell markers CD11b and CD33 in human tissues,²⁴ and the counterpart in mice is characterized by CD11b and Gr-1.²⁵ MDSCs can be divided into 2 groups: granulocytic MDSCs (G-MDSCs) and monocytic MDSCs (M-MDSC). Activated MDSCs inhibit

*Authors share co-first authorship.

Abbreviations used in this paper: CFSE, carboxyfluorescein succinimidyl ester; c-Myc, MYC proto-oncogene; COAD, colon adenocarcinoma; CRC, colorectal cancer; CRISPR/Cas9, Clustered regularly interspaced short palindromic repeats /CRISPR-associated protein 9; CSC, cancer stem cell; CXCL, C-X-C motif ligand; CXCR2, chemokine C-X-C motif receptor 2; DCLK1, doublecortin-like kinase 1; ELISA, enzyme-linked immunosorbent assay; ERK, extracellular signal-regulated kinase; FBS, fetal bovine serum; GAPDH, glyceraldehyde-3-phosphate dehydrogenase; G-MDSC, granulocytic myeloid-derived suppressor cell; GO, Gene Ontology; IL, interleukin; ICB, immune checkpoint blockade; KEGG, Kyoto Encyclopedia of Genes and Genomes; Ki-67, Antigen Ki-67; MAPK, mitogen-activated protein kinase; MDSC, myeloid-derived suppressor cell; MSS, microsatellite stable; NK, natural killer; PBS, phosphate-buffered saline; RNA-seq, RNA sequencing; RT-PCR, Real-time polymerase chain reaction; SC, subcutaneously; TCGA, The Cancer Genome Atlas; TGF- β , transforming growth factor; TME, tumor microenvironment; WT, wild-type.

 Most current article

© 2022 The Authors. Published by Elsevier Inc. on behalf of the AGA Institute. This is an open access article under the CC BY-NC-ND license (<http://creativecommons.org/licenses/by-nc-nd/4.0/>).

2352-345X

<https://doi.org/10.1016/j.jcmgh.2022.10.013>

immune effector functions for tumor eradication, including cytotoxic T lymphocytes and NK cells, by producing arginase 1, nitric oxide synthase 2, and other immunosuppressive cytokines.^{25,26} Notably, MDSCs can inhibit CD8⁺ T-cell cytotoxicity against tumor cells, and promote inflammation-associated tumorigenesis.²⁷ Moreover, emerging evidence has shown that MDSCs appear to accumulate in premetastatic sites,²⁸ and the abnormal accumulation of circulating MDSCs is highly correlated with cancer stage, metastasis, and survival in CRC and other gastrointestinal cancer patients.^{29–33} Currently, immunotherapy targeting MDSCs is considered to be one of the most promising investigational therapeutic avenues, with many preclinical experiments and clinical trials ongoing.

In this study, we explore the regulatory role of DCLK1 in the immune microenvironment of CRC development. We show that the expression of DCLK1 promotes the expression and secretion of the key tumorigenic chemokine CXCL1 in CRC cells. In turn, CXCL1 binds to chemokine C-X-C motif receptor 2 (CXCR2) on MDSCs and recruits them to the tumor microenvironment. The infiltration of MDSCs alters the local immune microenvironment, resulting in suppression of CD4⁺ T-cell and CD8⁺ T-cell proliferation and function, facilitating unhampered tumor growth and subsequent metastasis. In brief, we found the CSC marker DCLK1 actually can modulate tumor immunity through the recruitment of immunosuppressive MDSCs, and we may tackle the immune-privileged tumor microenvironment by targeting DCLK1.

Results

DCLK1 Knockout Leads to Elimination of Colorectal Cancer Cells in Immune-Competent Hosts

To explore the role of DCLK1 in tumor immune regulation, we chose DCLK1-expressing mouse colon cancer cells MC38 (C57BL/6J) and CT26 (BALB/c) and used Clustered regularly interspaced short palindromic repeats (CRISPR) technology to establish DCLK1-deficient lines. We implanted 1×10^6 DCLK1^{wild-type} (WT) or DCLK1^{-/-} cells subcutaneously (SC) into the flank of immune-deficient mice or immune-competent mice to investigate the functional interactions between tumor DCLK1 and the immune system. The result showed that in immune-deficient BALB/c nude mice, tumor growth of MC38 DCLK1^{WT} and DCLK1^{-/-} showed no obvious differences, suggesting that DCLK1 has minimal impact on the growth rate of MC38 and CT26 cells in the absence of immune surveillance. On the contrary, in immune-competent mice, MC38 DCLK1^{-/-} tumors showed nominal growth early on followed by gradual clearance, achieving complete regression at the end point, while the MC38 DCLK1^{WT} tumor growth remained normal and unaltered (Figures 1A and B and 2A). The result was repeated in DCLK1^{-/-} CT26 in WT BALB/c mice (Figures 1C and D and 2C). On day 21, we excised and weighed the tumors from DCLK1^{WT} and DCLK1^{-/-} groups, and found a significant difference between the 2 groups (Figure 2B and D). These results indicate that DCLK1 is necessary for tumor growth in

the presence of a functioning immune system and plays an important role in tumor immune escape.

To simulate in situ tumor growth, we injected DCLK1^{WT} and DCLK1^{-/-} cells into the intestine of C57BL/6J or BALB/c mice. In immunocompetent C57BL/6J mice, the tumor formation ratio was significantly higher in the MC38 DCLK1^{WT} group compared with the DCLK1^{-/-} group, although tumor growth was still small in 2 of the mice in the DCLK1^{WT} group (numbered 4 and 5). Overall, tumors formed in 5 of 9 mice in the DCLK1^{WT} group, but only 1 of 9 mice in the DCLK1^{-/-} group (Figure 1E). In situ tumor injection in the immunocompetent BALB/c mice showed similar results. That is, we found 5 of 8 mice developed multiple tumors in the CT26 DCLK1^{WT} group, whereas only 1 of 8 mice developed a single tumor in the DCLK1^{-/-} group (Figure 1F), indicating that the DCLK1 molecule is crucial for in situ colon tumor formation.

Adaptive immunity is characterized by recall responses.³⁴ We reasoned that if the enhanced rejection of DCLK1^{-/-} cells is indeed a consequence of host adaptive immune activation, their inoculation may be associated with immune memory. To confirm this hypothesis, we implanted C57BL/6J mice and BALB/c mice with syngeneic MC38 DCLK1^{-/-} or CT26 DCLK1^{-/-} cells SC, respectively. On day 21, the DCLK1^{-/-} tumor cells were completely cleared. We rechallenge the mice with DCLK1^{WT} or DCLK1^{-/-} tumor cells on day 28. The result showed that both DCLK1^{WT} and DCLK1^{-/-} cells failed to establish tumors (Figure 1G and H). These results indicate that the lack of DCLK1 promotes a host adaptive immune response with a typical recall response, providing evidence for an immunosuppressive function for DCLK1 in the context of tumorigenesis.

DCLK1 Ablation Promotes CRC Regression by Modulating MDSC Recruitment and T-Cell Activation

To further dissect the role of DCLK1 in host immunity, we decided to characterize the role of adaptive immune cells in DCLK1^{-/-} tumor regression. On day 7 after inoculation, we performed flow cytometry analysis of lymphocytes in tumor tissues. Results showed no obvious difference between total CD45⁺ and CD4⁺ T cells (Figure 3A and B). In contrast, we found that the infiltration of CD4⁺CD62L⁻CD44⁺ effector T cells increased in MC38 DCLK1^{-/-} tumors (Figure 3C and F), while the infiltration of CD8⁺ T cells increased significantly both in MC38 and CT26 DCLK1^{-/-} tumors (Figure 3D). Infiltration of CD8⁺CD62L⁻CD44⁺ T cells also increased significantly in MC38 DCLK1^{-/-} tumors (Figure 3E and F). Moreover, the proliferation of CD8⁺ T cells in the MC38 DCLK1^{WT} tumor was comparatively less robust, as indicated by reduced Ki-67 positivity. No significant difference in the Ki-67 index of CD4⁺ T cells was detected between DCLK1^{WT} and DCLK1^{-/-} tumors (Figure 3G). In addition, staining of CD8⁺ T cells in frozen sections from DCLK1^{WT} and DCLK1^{-/-} tumor tissues also showed noticeably increased infiltration in the DCLK1^{-/-} group (Figure 3H).

To further probe if there were any qualitative differences between CD4⁺ T cells and CD8⁺ T cells associated

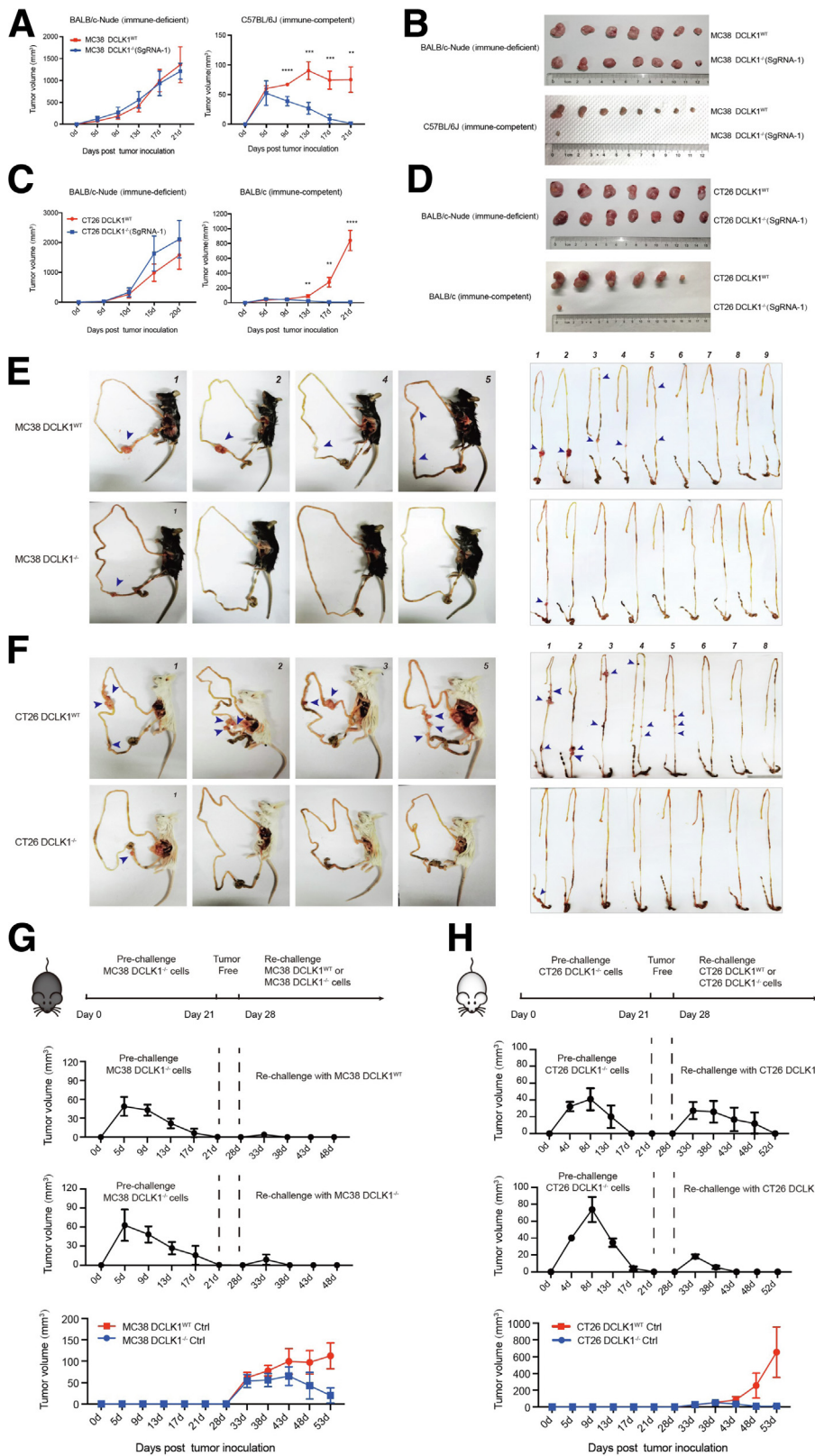


Figure 1. DCLK1 promotes tumor progression through immune escape. (A) Tumor growth of MC38-DCLK1^{WT} and MC38-DCLK1^{-/-} CRC cells implanted in immune-deficient nude mice and immune-competent C57BL/6J mice. (B) Photograph of subcutaneous tumor formation in the BALB/c nude and C57BL/6J mouse model. (C) Tumor growth of CT26-DCLK1^{WT} and CT26-DCLK1^{-/-} CRC cells implanted in immune-deficient nude mice and immune-competent BALB/c mice. (D) Photograph of subcutaneous tumor formation in the BALB/c nude and BALB/c mouse model. (E) CRC MC38-DCLK1^{WT} (top) and MC38-DCLK1^{-/-} (bottom) cells in situ transplantation into the intestine of C57BL/6 mice. Representative photographs of intestinal tumorigenesis (left panel) and anatomic photographs (right panel) as indicated (The arrowheads indicates the site of intestinal tumor formation). (F) CRC CT26-DCLK1^{WT} (top) and CT26-DCLK1^{-/-} (bottom) cells in situ transplantation into the intestine of BALB/c mice. Representative photographs of intestinal tumorigenesis (left panel) and anatomic photos (right panel) as indicated (The arrowheads indicates the site of intestinal tumor formation). (G) Tumor rechallenge of CRC MC38-DCLK1^{WT} (top) and MC38-DCLK1^{-/-} (middle) cells after pre-challenge of MC38-DCLK1^{-/-} cells in C57BL/6J mice. Subcutaneous growth of CRC MC38-DCLK1^{WT} and MC38-DCLK1^{-/-} tumors injected on day 28 without prechallenge (bottom) set as control. (H) Tumor rechallenge of CRC CT26-DCLK1^{WT} (top) and CT26-DCLK1^{-/-} (middle) cells after pre-challenge of CT26-DCLK1^{-/-} cells in BALB/c mice. Subcutaneous growth of CRC CT26-DCLK1^{WT} and CT26-DCLK1^{-/-} tumors were injected on day 28 without prechallenge (bottom) as in panel G. Data are presented as means ± SD; n = 6–9 tumors for each group. **P < .01, ***P < .001, and ****P < .0001, 2-tailed Student t test.

with tumor DCLK1, we analyzed the expression of co-inhibitory surface markers programmed death 1 and cytotoxic T lymphocyte A-4 on T cells. We failed to find

any indication of altered T-cell exhaustion marker expression (Figure 4A and B). In addition, we found no difference in Natural killer (NK) or Natural killer T (NKT)

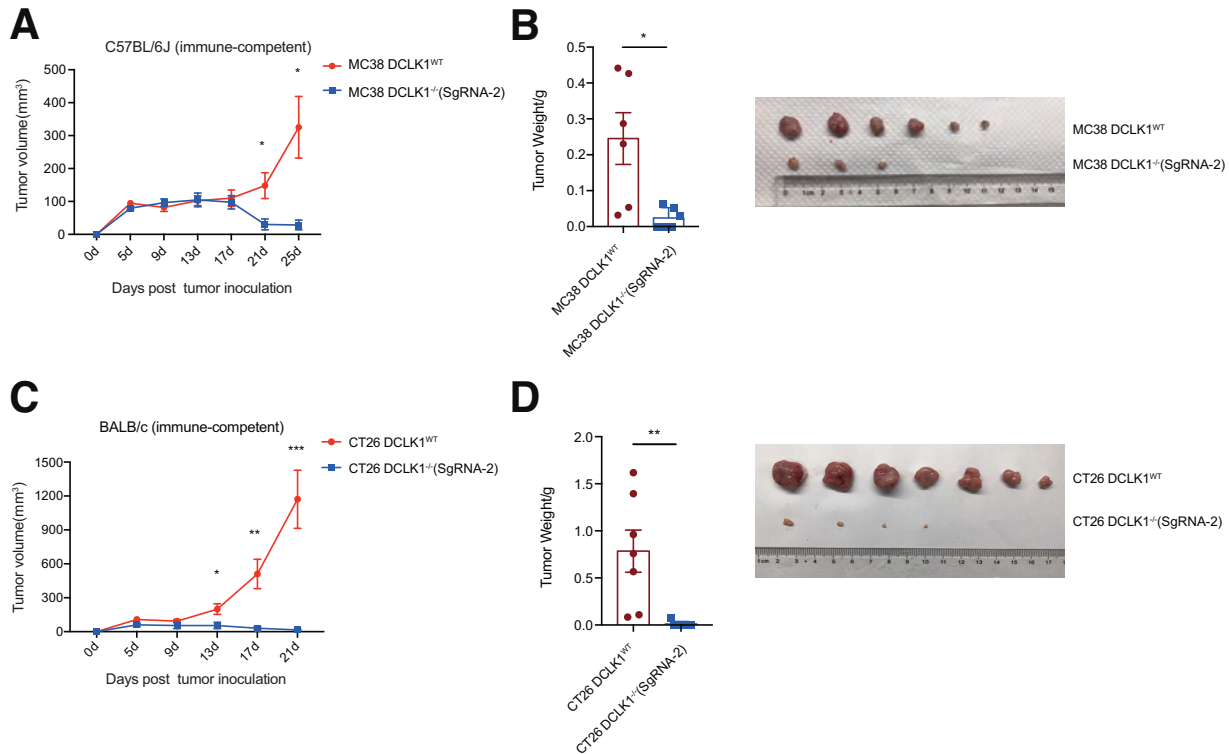


Figure 2. Loss of DCLK1 in tumor cells inhibits tumor growth *in vivo*, related to Figure 1. (A and B) Deletion of DCLK1 in the MC38 cell line inhibits tumor growth *in vivo*. (A) MC38-DCLK1^{WT} and single-guide RNA (SgRNA) #2 of MC38-DCLK1^{-/-} cells were injected into C57BL/6J mice. (B) Tumor weight was determined on the 21st day after transplantation and photograph shows subcutaneous MC38 tumor formation in a C57BL/6J mouse model. (C and D) Deletion of DCLK1 in the CT26 cell line inhibits tumor growth *in vivo*. (C) CT26-DCLK1^{WT} and SgRNA #2 of CT26-DCLK1^{-/-} cells were injected into BALB/c mice. (D) Tumor weight was determined on the 21st day after transplantation and photograph shows subcutaneous CT26 tumor formation in a BALB/c mouse model. Data are represented as means \pm SD; $n = 6-7$ tumors for each group. * $P < .05$, ** $P < .01$, and *** $P < .001$, 2-tailed Student t test.

cells (Figure 4C and D). Together, these data suggest that differences in infiltrating T cells between DCLK1^{WT} and DCLK1^{-/-} tumor implantations may explain the variable outcomes in DCLK1^{WT} and DCLK1^{-/-} tumor regression.

To validate the role of CD4⁺ and CD8⁺ T cells in DCLK1^{-/-} CRC tumor regression, we depleted CD4⁺ or CD8⁺ T-cell populations by neutralization antibody in mice bearing DCLK1^{-/-} MC38 tumor (Figure 5A and B), and found that removal of either type of T cells led to robust tumor growth exceeding the WT DCLK1 tumor in the control group (Figure 5C). Based on this, we tentatively concluded that the DCLK1^{WT} tumors escape immune surveillance via limiting the infiltration of CD4⁺ and CD8⁺ T cells. Subsequently, we assessed the activation status of CD8⁺ T cells. We found that the interferon- γ and granzyme B-positive T cell percentage of the total CD8⁺ T cells doubled in MC38 and CT26 DCLK1^{-/-} tumors, suggesting that DCLK1 knockout boosted the activation intensity of individual CD8⁺ T cells (Figure 6A and B). Together, these findings provide direct functional proof that CD4⁺ and CD8⁺ T cells are responsible for the regression of DCLK1^{-/-} tumors.

Mounting evidence has suggested that the accumulation of MDSCs in the tumor microenvironment can inhibit the infiltration and function of T cells and promote the

immune escape of tumors.^{21,35-37} Next, we analyzed immunosuppressive cell infiltration in DCLK1^{WT} and DCLK1^{-/-} tumors. As shown by the flow cytometry results, there was a significant decrease in G-MDSC infiltration in the DCLK1^{-/-} group (Figure 6C and D). Subsequently, to clarify whether DCLK1 regulates the MDSC function besides recruitment, we detected the expression of arginase-1 and nitric oxide synthase 2, which suppress T-cell function.^{36,37} As shown by the results, these 2 immunosuppressive molecules show similar intensity between DCLK1^{WT} and DCLK1^{-/-} groups (Figure 6E). Furthermore, to determine whether MDSCs from these 2 groups impede T-cell proliferation, we isolated the mouse spleen CD8⁺ T cells, labeled with carboxyfluorescein succinimidyl ester (CFSE) and stimulated with anti-CD3 and anti-CD28 antibody in the presence of equal numbers of MDSCs sorted from mouse subcutaneous MC38 DCLK1^{WT} and DCLK1^{-/-} tumors. MDSCs from DCLK1^{WT} and DCLK1^{-/-} groups showed similar inhibition of T-cell proliferation *in vitro* (Figure 6F). However, because MDSC infiltration in the DCLK1^{-/-} CT26 tumor is severely defective, we did not acquire enough MDSCs from CT26 tumors. These results indicate that MDSCs from DCLK1^{WT} tumors do not possess more potent T-cell inhibition than DCLK1^{-/-} tumors. In brief, these results implicate positive regulation

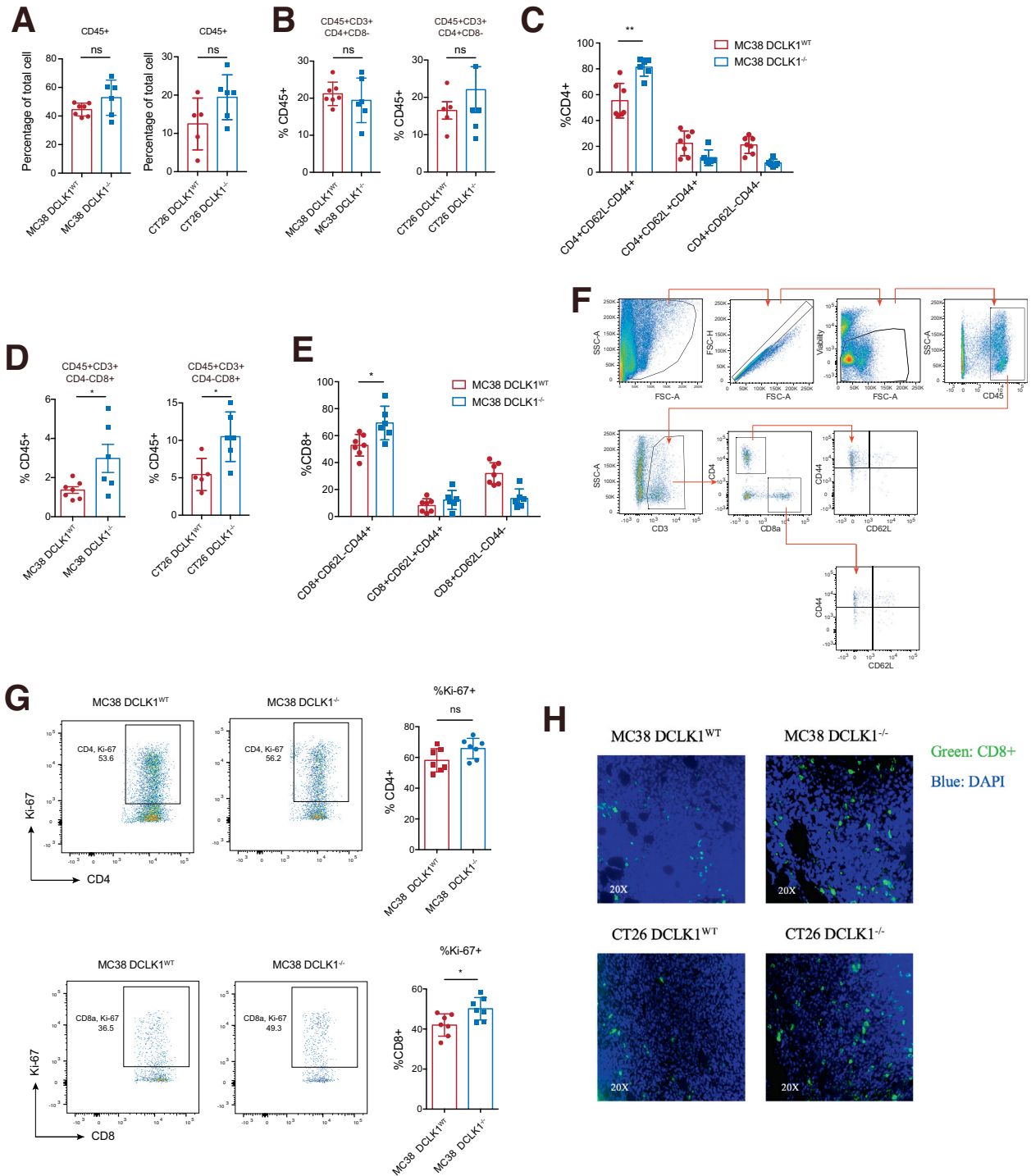


Figure 3. DCLK1-depleted tumors show increased T-lymphocyte infiltration. (A) Flow cytometry quantification of CD45⁺ cell infiltration in CRC DCLK1^{WT} and CRC DCLK1^{-/-} group intratumor tissues. (B) Flow cytometry quantification of total CD4⁺ T-cell infiltration in CRC DCLK1^{WT} and CRC DCLK1^{-/-} group intratumor tissues. (C) Flow cytometry quantification of effector CD4⁺ T-cell (CD4⁺CD44⁺CD62L⁻) infiltration in MC38-DCLK1^{WT} and MC38-DCLK1^{-/-} group intratumor tissues. (D) Flow cytometry quantification of CD8⁺ T-cell infiltration in CRC DCLK1^{WT} and CRC DCLK1^{-/-} group intratumor tissues. (E) Flow cytometry quantification of effector CD8⁺ T-cell (CD8⁺CD44⁺CD62L⁻) infiltration in MC38-DCLK1^{WT} and MC38-DCLK1^{-/-} group intratumor tissues. (F) Flow cytometry gating strategy applied for identification of T-cell subpopulations. (G) Flow cytometry quantification of Ki-67⁺ cells as a percentage of infiltrating CD4⁺ and CD8⁺ T cells. (H) Frozen sections from MC38-DCLK1^{WT}, MC38-DCLK1^{-/-} and CT26-DCLK1^{WT}, CT26-DCLK1^{-/-} subcutaneous tumor tissues were subjected to immunostaining analysis for CD8a (green) along with 4',6-diamidino-2-phenylindole (DAPI) for DNA (blue). Data are presented as means ± SD; n = 5–7 tumors for each group. For frozen section staining, 3 sections were stained for each group of tumors. *P < .05, **P < .01, 2-tailed Student *t* test. CD44⁺CD62L⁻, effector T cells; CD44⁺CD62L⁺, central memory T cells; CD44⁻CD62L⁺, naïve T cells; FSC-A, Forward Scatter-Area; SSC-A, Side Scatter-Area.

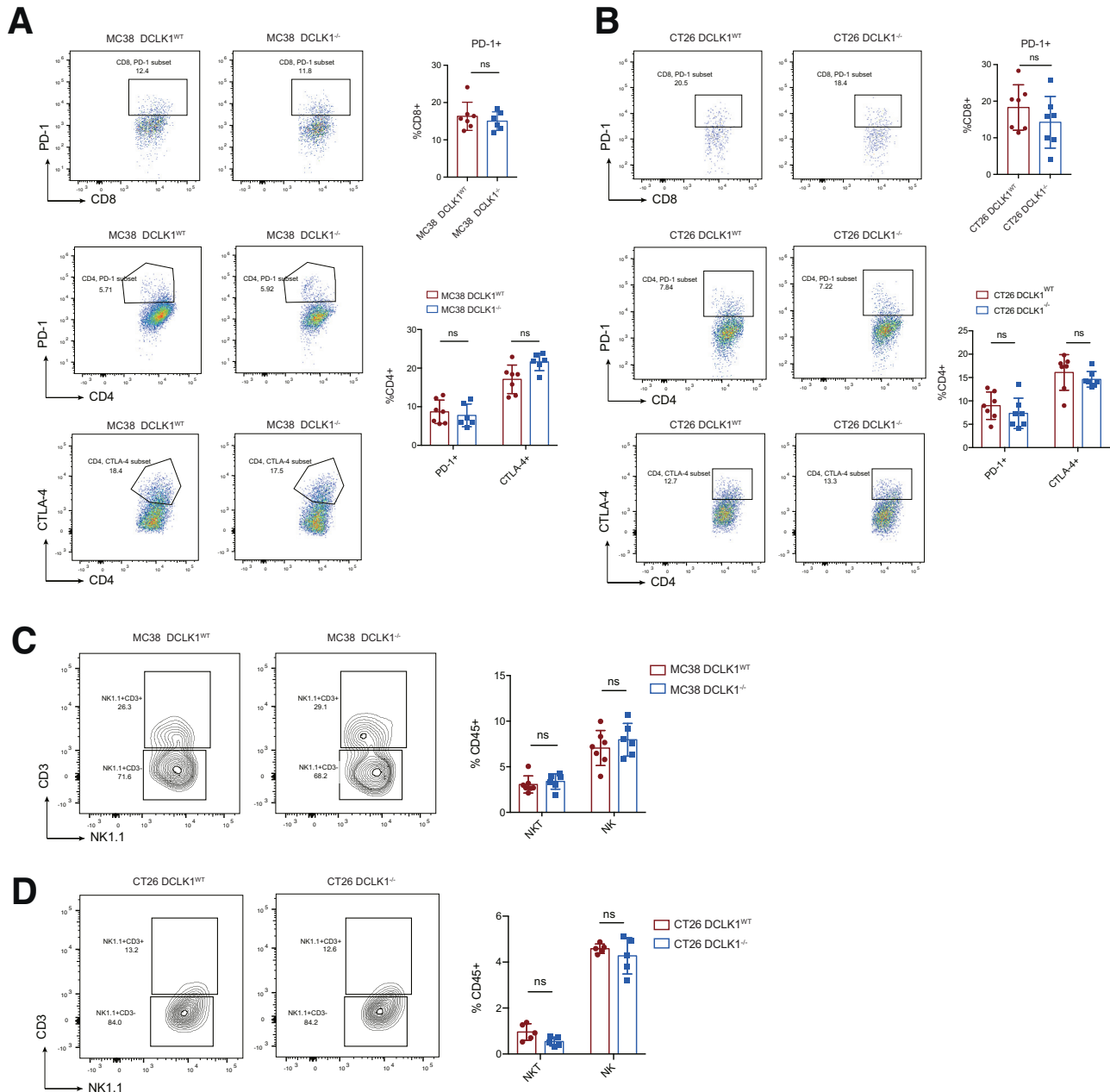


Figure 4. DCLK1 deletion boosts antitumor immunity independent of T-cell exhaustion and NK cell infiltration. Flow cytometry quantification of inhibitory marker, including programmed death 1 (PD-1) and cytotoxic T lymphocyte (CTL)A-4, by the percentage of CD8⁺ and CD4⁺ tumor-infiltrating T cells in (A) CRC MC38-DCLK1^{WT}, MC38-DCLK1^{-/-} group intratumor tissues, and (B) CRC CT26-DCLK1^{WT}, CT26-DCLK1^{-/-} group intratumor tissues. Flow cytometry quantification of Natural Killer (NK) cells and (Natural Killer T) NKT cells infiltrating (C) MC38-DCLK1^{WT}, MC38-DCLK1^{-/-} group intratumor tissues and (D) CT26-DCLK1^{WT}, CT26-DCLK1^{-/-} group intratumor tissues. Data are presented as means \pm SD; n = 5–7 tumors for each group, 2-tailed Student *t* test.

of G-MDSC recruitment in DCLK1-expressing tumors, but no alteration on the T-cell inhibitory capacity of MDSCs.

MDSC-Recruiting Chemokines, CXCL1 and CXCL2, Are Highly Expressed in DCLK1^{WT} CRC Tumor Cells

To explore the mechanism of increased intratumoral MDSCs in DCLK1-expressing tumors, we performed the RNA

sequencing (RNA-seq) analysis of MC38 DCLK1^{WT} and DCLK1^{-/-} cells. Kyoto Encyclopedia of Genes and Genomes (KEGG) and Gene Ontology (GO) enrichment analysis identified remarkable differences in the mitogen-activated protein kinase (MAPK)/extracellular signal-regulated kinase (ERK) pathway between DCLK1^{WT} and DCLK1^{-/-} tumors (Figure 7A and B). Correlation analysis of the RNA-seq results showed that genes in the ERK pathway are correlated with DCLK1 (Figure 7C). Next, we confirmed that DCLK1 expression is

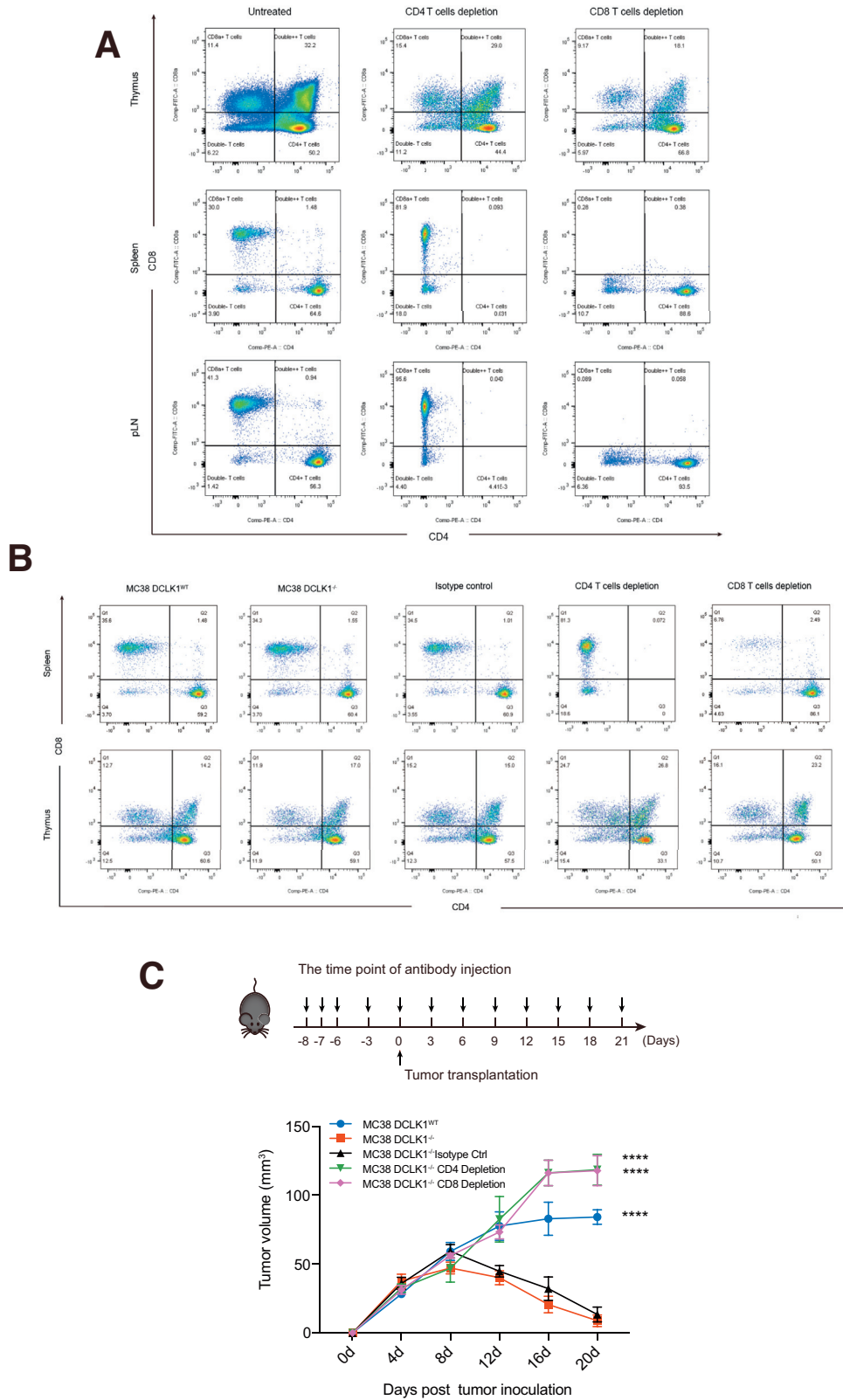
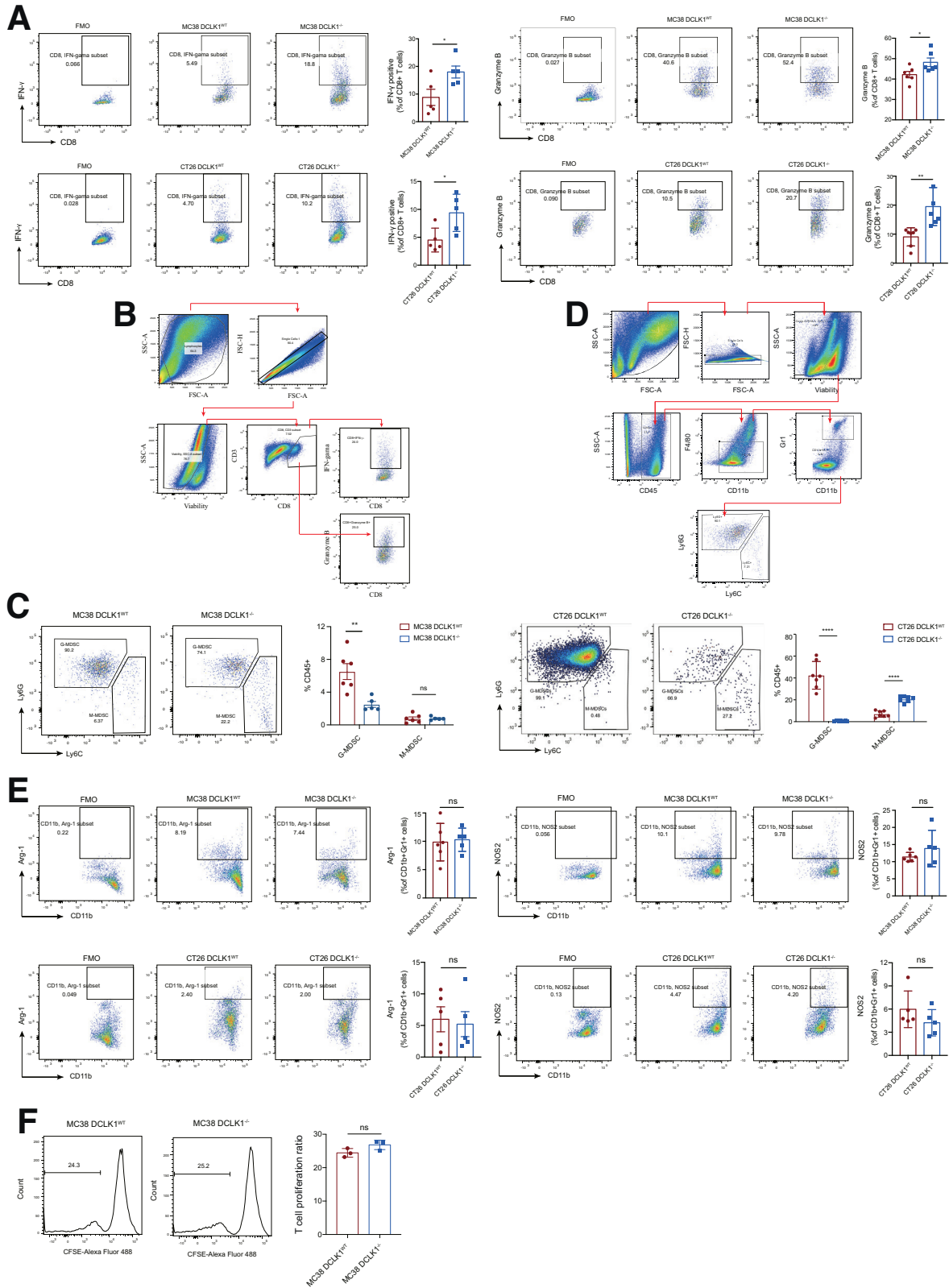


Figure 5. CD4+ T and CD8+ T cells are responsible for the clearance of DCLK1^{-/-} tumor cells. (A) Flow cytometry analysis of antibody-mediated T-cell depletion. T-cell populations of spleen, lymph node, and thymus tissue from mice commencing 8-day neutralizing antibody treatment before tumor inoculation. (B) Flow cytometry examination of T-cell populations of spleen and thymus tissue from tumor-bearing animals with continuing T-cell depletion antibody treatment. (C) Tumor growth kinetics after transplantation of CRC MC38-DCLK1^{WT} or MC38-DCLK1^{-/-} cells into C57BL/6J mice receiving anti-CD4 or anti-CD8a neutralizing antibodies. n = 6–8 tumors for each group, 2-tailed Student *t* test, *****P* < .0001. Ctrl, control; PE-A, Phycoerythrin-Area.

correlated positively to ERK pathway activation in human CRC through analysis of the colorectal adenocarcinoma (COAD) The Cancer Genome Atlas (TCGA) cohort (Figure 7D).

According to recent studies, CXCL1 and CXCL2 are both ligands of CXCR2 and play an important role in G-MDSC recruitment.^{27,38} Notably, CXCL1 and CXCL2 dramatically



decreased in the DCLK1^{-/-} group (Figure 7E). Furthermore, search tool for recurring instances of neighboring genes (STRING) based protein-protein interaction analysis suggested a relationship between DCLK1 and CXCL1 and CXCL2 through the ERK pathway (Figure 7F).

To verify the results of the transcriptome analysis, we examined the expression of CXCR2 ligands by Real-time polymerase chain reaction (RT-PCR). CXCL1 and CXCL2 expression were markedly higher in MC38 or CT26 DCLK1^{WT} cells compared with DCLK1^{-/-} cells (Figure 7G and J). To further confirm these results in human CRC lines, we selected SW480 with high expression of DCLK1, and HCT116 with low expression of DCLK1. After knocking out or overexpressing DCLK1 in these 2 CRC lines, respectively, we tested the expression of CXCL1 and CXCL2 and found decreased expression of both in SW480 DCLK1^{-/-} CRC lines (Figure 7K). Conversely, when we forced the expression of DCLK1 in HCT116 cells, the expression of CXCL1 and CXCL2 increased (Figure 7M). We further confirmed the CXCL1 and CXCL2 expression in cell culture supernatant using enzyme-linked immunosorbent assay (ELISA). Protein levels of CXCL1 and CXCL2 in DCLK1^{-/-} medium were lower than those in DCLK1^{WT} medium, whereas DCLK1 overexpression led to higher levels (Figure 7H, J, L, and N). These data together show that the expression of chemokines CXCL1 and CXCL2, which are known to recruit MDSCs, are regulated by DCLK1. To prove that DCLK1 regulates MDSC recruitment by promoting the expression of CXCL1 and CXCL2, we extracted MC38 and CT26 tumor tissues inoculated SC in mice, isolated MDSCs, and cultured them in a Transwell upper chamber. The conditioned medium of DCLK1^{WT} and DCLK1^{-/-} tumor cells were added to the lower chamber and the migratory ability of MDSCs was detected. MDSC migration in the DCLK1^{WT} conditioned medium was increased significantly compared with the DCLK1^{-/-} group (Figure 7O). These data show that DCLK1 promotes the expression of chemokines CXCL1 and CXCL2, which are known to recruit MDSCs in the tumor microenvironment.

DCLK1 Induces CXCL1/CXCL2 Expression via the ERK Pathway

The earlier-described results indicate that the expression of CXCL1 and CXCL2 is regulated by the expression of

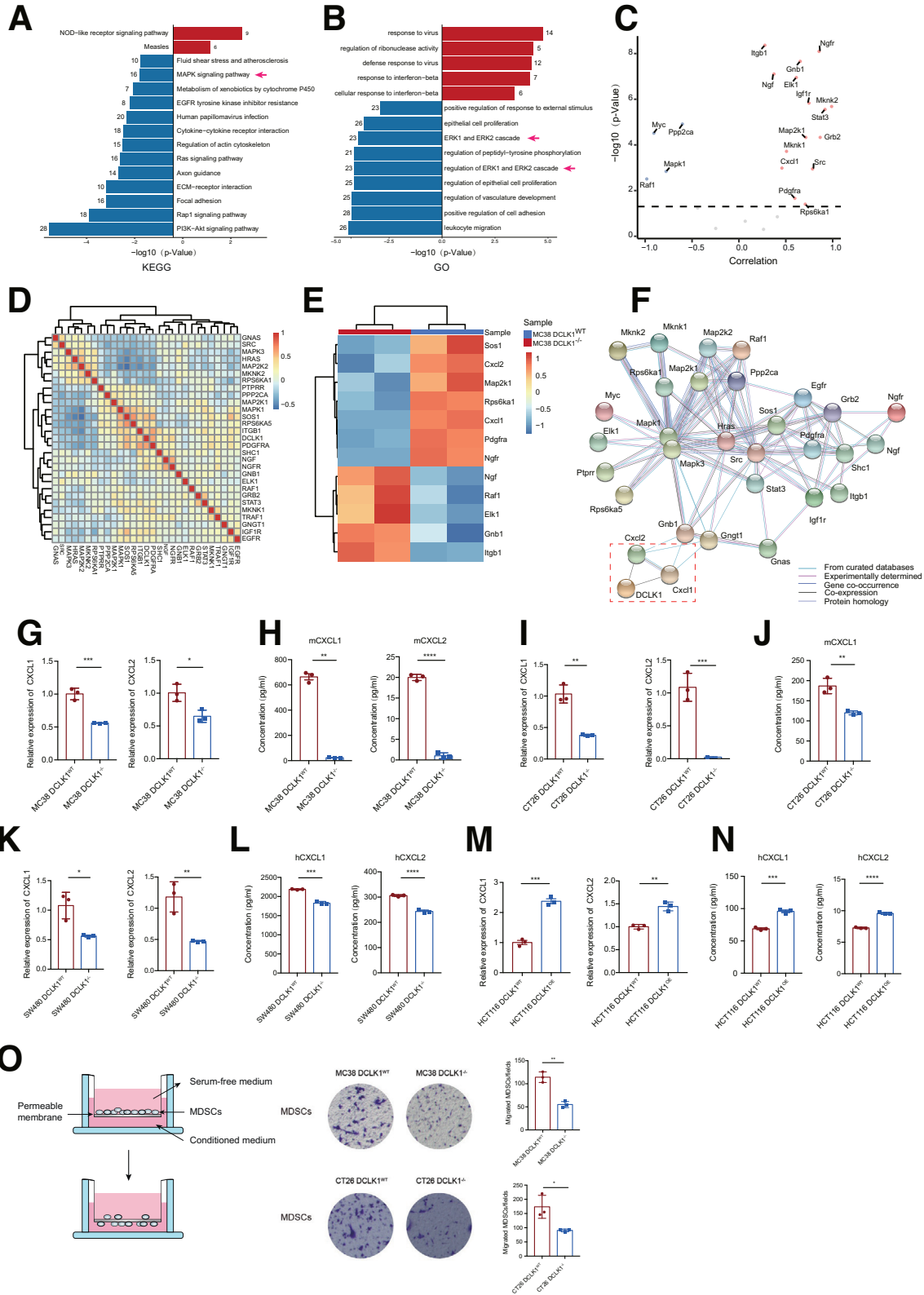
DCLK1. Because we found remarkable differences in ERK pathway enrichment in the DCLK1^{WT} group compared with the DCLK1^{-/-} cell lines, we sought to assess this finding at the protein level. Western blot showed significantly decreased ERK phosphorylation in DCLK1^{-/-} tumor cells (Figure 8A). To further investigate whether DCLK1 regulates CXCL1 and CXCL2 through the ERK pathway, we used ERK-specific inhibitor SCH772984³⁹ to treat MC38, CT26, SW480, and DCLK1-overexpressing HCT116 cells, and detected the expression changes of CXCL1 and CXCL2 by RT-PCR. The expression of CXCL1 and CXCL2 noticeably decreased after inhibition of the ERK pathway by SCH772984 (Figure 8B). According to the Eukaryotic Promoter Database (EPD) (<https://epd.epfl.ch//index.php>) generated from validated experimental results, we found that MYC proto-oncogene (c-Myc), a key downstream transcription factor of the ERK pathway,^{40,41} has specific binding sites on the promoter of CXCL1 and CXCL2. Next, we detected the expression of c-Myc in the nucleus. The results showed that there was a positive correlation between the expression of c-Myc and DCLK1 in the nucleus (Figure 8C).

To further explore the function of CXCL1 and CXCL2 in DCLK1+ tumors, we rescued the expression of CXCL1 and CXCL2 in the DCLK1^{-/-} MC38 cell line and transplanted the DCLK1^{WT}, DCLK1^{-/-}, DCLK1^{-/-}-CXCL1^{OE}, and DCLK1^{-/-}-CXCL2^{OE} cell lines into the flanks of C57BL/6J mice. CXCL1 rescue led to a tumor growth rate for DCLK1^{-/-} CRC cells similar to WT cells. However, tumor growth was not restored by CXCL2 overexpression (Figure 8D). Notably, the rescue of CXCL1 also reduced the infiltration of CD8⁺ T cells and enhanced the infiltration of MDSCs (Figure 8E). To validate this, we established an in situ mouse model of intestinal tumor and found that MC38 DCLK1^{WT} cells had the highest rate of tumorigenesis, including 2 of 6 mice showing a heavy tumor burden (tumor size, >5 mm), 2 mice with moderate burden (tumor size, 2–4 mm), and 1 mouse with mild tumor burden (tumor size, 1–2 mm). In contrast, only 2 mice in the DCLK1^{-/-} group had visible tumors, and the tumor burden was relatively low (tumor size, 1–2 mm). As expected, CXCL1 (but not CXCL2) overexpression in DCLK1^{-/-} tumors led to exceeding in situ tumor growth and 5 of 6 mice developed multiple tumors, the tumors of mice 1–3 were more than 5 mm in diameter, and mice 4

Figure 6. (See previous page). DCLK1-expressing tumors show a higher proportion of MDSC infiltration, which inhibits T-cell proliferation. (A) Flow cytometry quantification of CD8⁺IFN- γ ⁺ cell and CD8⁺GranzymeB⁺ cell percentage in CRC DCLK1^{WT} and DCLK1^{-/-} subcutaneous tumors from immunocompetent mice (*top panel*: MC38-DCLK1^{WT}, MC38-DCLK1^{-/-} groups; *bottom panel*: CT26-DCLK1^{WT}, CT26-DCLK1^{-/-} groups). (B) Flow cytometry gating strategy for IFN- γ and GranzymeB staining of CD8⁺ T cells applied for identification of the CD8⁺ T-cell activation status. (C) Representative flow cytometry quantification of the MDSC subpopulation in MC38-DCLK1^{WT} and MC38-DCLK1^{-/-} group intratumor tissues (*left panel*), and CT26-DCLK1^{WT} and CT26-DCLK1^{-/-} group intratumor tissues (*right panel*). (D) Flow cytometry gating strategy applied for identification of the MDSC subpopulation. Ly6G⁺ subpopulation, (G-MDSCs); Ly6C⁺ subpopulation, monocytic MDSC (M-MDSC). (E) Representative flow cytometry quantification of arginase 1 (ARG-1) (*left*) and nitric oxide synthase 2 (NOS2) (*right*) percentage of MDSCs in MC38-DCLK1^{WT} and MC38-DCLK1^{-/-} group intratumor tissues (*upper panel*), and CT26-DCLK1^{WT} and CT26-DCLK1^{-/-} group intratumor tissues (*lower panel*). (F) Flow cytometry results of the CFSE-labeled T-cell proliferation. CD8⁺T cells, activated by anti-CD3/28 (4 μ g/mL), were co-cultured with MDSCs sorted from the subcutaneous MC38 DCLK1^{WT} and DCLK1^{-/-} tumors. The proliferation of CD8⁺ T cells is indicated by percentage. Data are presented as means \pm SD; n = 5–7 tumors for each group. **P* < .05, ***P* < .01, and *****P* < .0001, 2-tailed Student *t* test. FMO, _Fluorescence Minus One; FSC-H, Forward Scatter-Height; IFN, interferon; SSC-A, _Side Scatter-Area.

and 5 were approximately 3 mm in diameter, which was consistent with the subcutaneous tumor transplantation assays. In agreement with the subcutaneous tumorigenesis

assay, DCLK1^{-/-}-CXCL2^{OE} inoculation had no such effect, indicating the dominant role of CXCL1 in DCLK1-mediated tumorigenesis (Figure 8F).



CXCR2 has been implicated in the progression of a wide range of tumor types.^{42,43} Recent research reported that antagonists targeting CXCR2 showed efficacy in inflammatory response and against colorectal tumors.⁴⁴ To examine whether modulation of CXCR2 alters MDSC recruitment to the tumor microenvironment, we administered the CXCR2 antagonist (SB265610) to DCLK1^{WT} MC38 tumor-bearing mice. It showed that administration of CXCR2 antagonist efficiently inhibited tumorigenesis of DCLK1^{WT} cells (Figure 8G), along with promoted infiltration of CD8+ T cells; the infiltration of MDSCs, however, was suppressed accordingly (Figure 8H). We investigated the antitumor effect of SB265610 with the in situ model of DCLK1 cells. We found that intestinal tumorigenesis in DCLK1^{WT} cell transplanted mice remained severe, 3 mice showed 3- to 4-mm diameter tumor formation, and the other 3 mice showed 2- to 3-mm tumors, including 2 mice with multiple tumor formation. Tumor burden was milder in mice treated with SB265610, only 4 of the 6 mice had tumor formation with a diameter of 1–3 mm, and all developed individually. Because of the tumor-suppressive effect of DCLK1-knockout in situ, accurately assessing the inhibitory effect of SB265610 is not possible. However, in the DCLK1-knockout cell inoculated group, only 1 of 6 mice treated with SB265610 developed a tumor with a diameter of 1 mm, while 2 of 6 mice treated with vehicle developed tumors that were 2 mm in diameter (Figure 8I). Collectively, these findings suggest that CXCL1–CXCR2 interaction downstream of DCLK1 plays a critical role in the tumorigenesis and progression of DCLK1+ CRC.

Clinical Expression of DCLK1 and CXCL1 in CRC Patients and the Relevance of DCLK1 and MDSC Signature

Our findings indicate that DCLK1 can affect the tumor immune microenvironment by recruiting MDSCs and promoting tumor immune escape. To verify this in clinical samples, we analyzed the TCGA COAD cohort with an established MDSC gene signature,⁴⁵ and identified a strong positive

correlation with DCLK1 expression (Figure 9A). Notably, CD33, a classic marker of human MDSCs, showed a significant correlation with DCLK1 (Figure 9B). Using polychromatic fluorescent staining, we evaluated the expression of DCLK1, CXCL1, and CD33 in primary CRC and paracancerous tissues. The results showed that high expression of DCLK1 was accompanied by high expression of CD33 and an increased level of CXCL1 in colon cancer tissues compared with the DCLK1-low tumor tissues and adjacent tissues (Figure 9C).

We further clarified the prognostic value of DCLK1 in CRC patients of the TCGA COAD project and found that high DCLK1 expression significantly correlated to poor prognosis for stage I/II CRC patients. We speculate that the main reason for this may be DCLK1-mediated immunosuppression and the resulting effect on tumor recurrence and metastasis (Figure 9D). In addition, stage I patients with high expression of DCLK1 have a worse prognosis for overall survival than those with lower expression, and the hazard ratio was 8.081, suggesting that DCLK1 is a predictor for the overall survival of patients with stage I CRC, but high DCLK1 expression is not a good predictor of overall patient survival for the rest of the stages (Figure 9E). This finding suggests that the detection of DCLK1 expression can predict the survival of patients with early CRC, which may be of significance for clinical diagnosis and treatment.

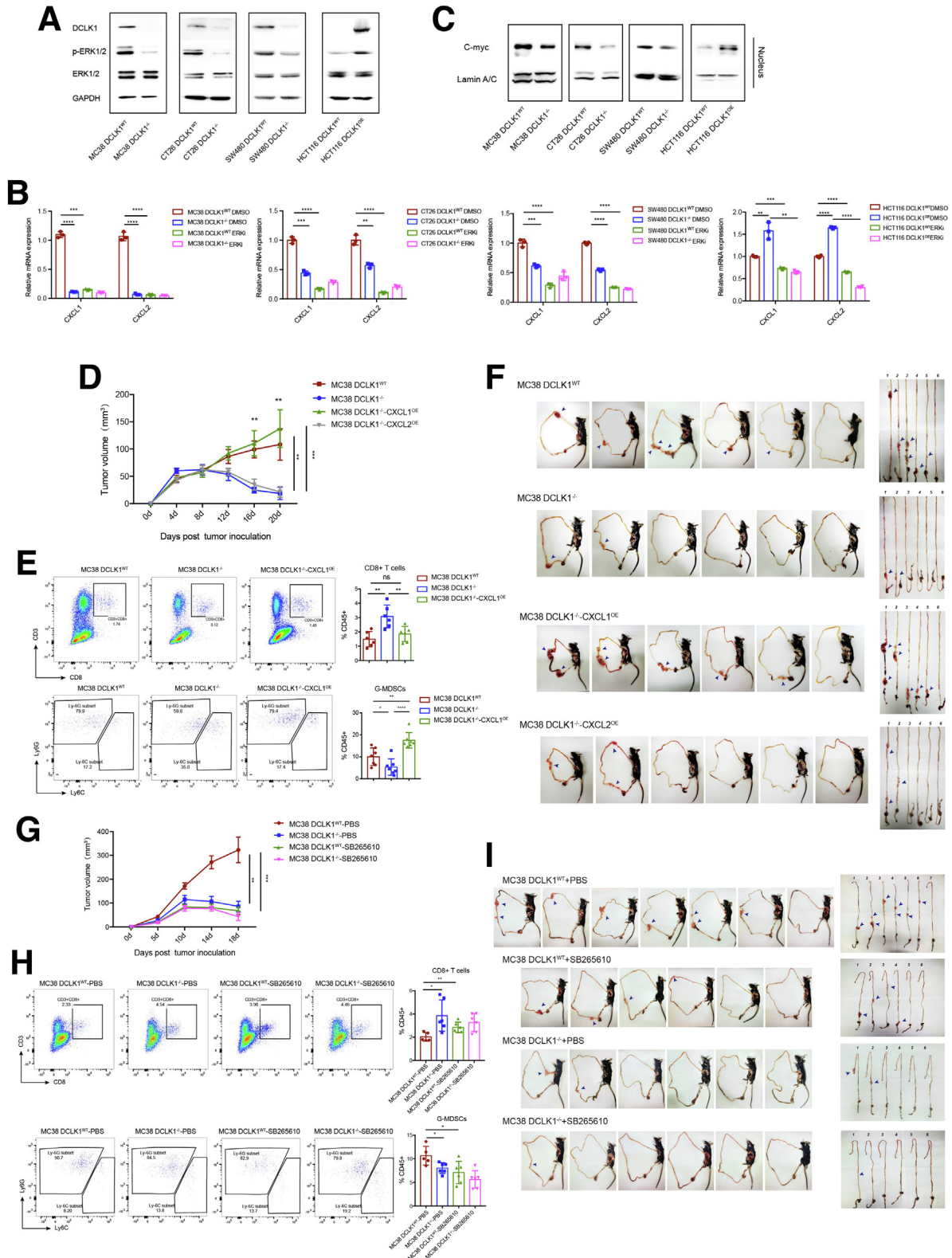
Discussion

DCLK1 is well known as a molecule that is highly expressed in CRC,^{13,15,46} pancreatic cancer,^{47,48} renal cancer, and other tumors.^{49,50} In various models and human samples, it regulates the development, progression, metastasis, and epithelial–mesenchymal transition of tumors. Studies have shown that inhibition of DCLK1 expression can slow down tumor progression and metastasis.^{14,49,51} We observed similar results consistent with previous studies, such as DCLK1 knockout impeded the tumor cell migration in MC38 and CT26 tumor cell lines (Figure 10A and B). However, some of our findings differed from previous studies. For example, we found no change in cell

Figure 7. (See previous page). The recruitment factors for MDSCs (CXCL1 and CXCL2) are highly expressed in DCLK1-high colon carcinoma. (A) KEGG analysis shows that genes affected by DCLK1 knockout are enriched in the MAPK–ERK pathway. (B) GO enrichment analysis suggests that down-regulated genes are enriched in processes related to Erk1 and Erk2 cascade. (A and B) Red bars indicate up-regulated genes, while blue bars indicate down-regulated genes. The numbers around the bars are the number of genes in corresponding categories. (C) Expression correlations between DCLK1 and genes in the MAPK–ERK pathway. The X-axis shows Pearson correlation coefficients, and the Y-axis shows $-\log_{10}$ (*P* values) for the correlations. (D) Co-expression relationships between DCLK1 and the MAPK–ERK pathway in TCGA-COAD project (*n* = 480). (E) Expression differences among genes in the MAPK–ERK pathway. Levels are normalized by row. (F) Co-expression relationships identified in this study suggest potential crosstalk between DCLK1 and the MAPK–ERK pathway via CXCL1/CXCL2. Nodes represent proteins, and edges represent protein–protein associations, whose colors represent levels of evidence. Relative messenger RNA expression levels of CXCL1 and CXCL2 in (G) MC38-DCLK1^{WT}, MC38-DCLK1^{-/-}, and (H) CT26-DCLK1^{WT}, CT26-DCLK1^{-/-} tumor cells and (I) human CRC cell lines SW480-DCLK1^{WT}, SW480-DCLK1^{-/-}, and (M) HCT116-DCLK1^{WT}, HCT116 DCLK1^{OE} by RT-PCR analysis. ELISA results of cell supernatants of (H and J) CRC cell lines MC38-DCLK1^{WT}, MC38-DCLK1^{-/-}, CT26-DCLK1^{WT}, and CT26-DCLK1^{-/-}, and (L and N) human CRC cell line SW480-DCLK1^{WT}, SW480-DCLK1^{-/-}, HCT116-DCLK1^{WT}, and HCT116 DCLK1^{OE}. (O) High expression of DCLK1 promotes MDSC recruitment *in vitro*. MC38 or CT26 cells were inoculated subcutaneously into WT C57BL/6J or BALB/c mice. On the seventh day, the tumor tissues were stripped and tumor-infiltrating MDSCs were isolated. MDSCs (2×10^5) were placed into the Transwell upper chamber. DCLK1^{WT} and DCLK1^{-/-} cell-conditioned medium were added into the lower chamber of the Transwell, and the migration of MDSCs was observed 48 hours later. Data are presented as means \pm SD. **P* < .05, ***P* < .01, ****P* < .001, and *****P* < .0001, 2-tailed Student *t* test. Akt, protein kinase B; ECM, Extracellular matrix; EGFR, Epidermal Growth Factor Receptor; NOD, Non Obese Diabetes; PI3K, Phosphoinositide-3-kinase.

proliferation between DCLK1^{WT} and DCLK1^{-/-} groups of mouse CRC cell lines (Figure 10C-F). Accordingly, there was no significant difference in *in vivo* tumor growth in immune-

deficient mice between the 2 groups (Figure 1A and C), which differed from previous results in human CRC cell lines.¹⁷ We also explored cell-cycle changes in DCLK1^{WT} and



DCLK1^{-/-} cell lines and found no alteration (Figure 10G and H). This observation is critical for our collective research on this molecule because the former would attribute the role of DCLK1 in cell-intrinsic regulation while our finding put this molecule front and center in host immune regulation.

In this study, we discovered that DCLK1 can lead to immunosuppression in CRC and promote tumor progression. By constructing *in situ* and subcutaneous tumor models of mouse intestinal cancer, comparing tumor formation in immunocompetent and immunodeficient mice, and combining differential analysis of tumor-infiltrating immune cells, we confirm the regulatory role of DCLK1 on inhibitory tumor microenvironment *in vivo*. We note that current studies on DCLK1-mediated tumor immune escape are based mainly on transcriptional or bioinformatic analysis and cell-level verification,^{52,53} but few studies have validated the immune modulation role of DCLK1 *in vivo*.

Immune escape plays an important role in tumor occurrence and development. A suspected role for DCLK1 in this process has been inferred from numerous reports.^{52,54} However, mechanistic insights remain elusive. In support of the immune-centric role of DCLK1, our team recently found that DCLK1 could promote the expression of programmed cell death-ligand 1 on pancreatic tumor cells via up-regulating the Yes associated protein1 (YAP1) molecule. YAP1 is a potent regulator of the Hippo pathway that is an integral part of host immunity.⁵⁵ Recent studies also have shown that DCLK1 is correlated with a variety of immune cells, including CD8⁺ T cells and CD4⁺ T cells in the CRC immune microenvironment.⁵² In our study, in addition to the close relationship between DCLK1, CD4⁺ T cells, and CD8⁺ T cells, we also found that DCLK1 plays a crucial role in the recruitment of immunosuppressive MDSCs, a key group of cells that have not been experimentally linked to DCLK1. MDSCs, a heterogeneous population of immature myeloid immune cells, have been reported to be indispensable for tumor angiogenesis, invasion, and metastasis.^{23,36,56} The CXCL-CXCR2 axis is required in the recruitment and trafficking of MDSCs. CXCL1, CXCL2, CXCL3,

and CXCL5 are all important ligands of CXCR2 and contribute to the infiltration of MDSCs into the colonic mucosa and tumors.^{27,57} In the TME, the accumulation of MDSC cells is one of the most important mechanisms of tumor immune escape, and targeting MDSCs is a promising therapeutic avenue.^{24,58} As for the mechanism of MDSC recruitment by DCLK1, our study found that activation of the MAPK/ERK pathway facilitates CXCL1 expression, and the c-Myc transcription factor downstream of ERK was found to have binding sites with the CXCL1 promoter, but whether additional pathways involved in the DCLK1-mediated regulation of CXCL1/2 remains to be determined. Therefore, the present findings are a vital supplement to the current studies, without which the reality of this phenomenon *in vivo* would remain unknown.

Immune checkpoint blockade (ICB) therapy is a major breakthrough in cancer treatment. However, at present, ICB is only highly applicable to non-small cell lung cancer, melanoma, and renal cancers. For patients with CRC, ICB shows promise only in the small subset of patients with damaged mismatch repair or microsatellite instability-high tumors.⁵⁹ In this study, we explored the role of DCLK1 with both microsatellite instability MC38 and MSS CT26 tumor cell lines and reached the same conclusion. Therefore, our study can be viewed as a mismatch repair-independent approach. In addition, many reports have indicated that CRC patients remain resistant to ICB. The possible mechanisms include the decrease in T-cell infiltration, the absence of tumor-specific antigens, and the increase in immunosuppressive cell infiltration.^{60,61} Recently, attention is being paid to MDSCs, which may be partly responsible for the failure of ICB treatment.^{62,63} The combination of MDSC-targeted drugs and ICB also has been performed in a number of clinical trials, such as NCT04599140. In this Clinical Trial, the efficacy of nivolumab in combination with the CXCR1/2-receptor antagonist SX-682 was evaluated in patients with MSS colon cancer, but the results have not yet been shown.

Collectively, we found that DCLK1 promotes the immunosuppressive TME through recruitment of MDSCs, and

Figure 8. (See previous page). DCLK1 regulates MDSC recruitment factor CXCL1 through the ERK pathway. (A) Immunoblot results of ERK protein phosphorylation in DCLK1-knockout MC38, CT26, and SW480 cells compared with control cells, and DCLK1-overexpressing HCT116 cells compared with control cells. (B) RT-PCR results for CXCL1 and CXCL2 in DCLK1^{WT}, DCLK1^{-/-} cells and DCLK1^{WT}, DCLK1^{OE} treated with or without SCH772984 (ERK inhibitor) (1 μmol/L, 48 hours). (C) Western blot results for nuclear protein extracts that have validated binding to the CXCL1 and CXCL2 promoter region. (D) Tumor growth in mice injected SC with DCLK1^{WT}, DCLK1^{-/-} cells, and CXCL1 or CXCL2 rescued DCLK1^{-/-} cells, the tumor-growth kinetics were measured every 4–5 days. (E) Flow cytometry quantification of CD8⁺ T cells and the MDSC percentage for subcutaneous MC38-DCLK1^{WT}, MC38-DCLK1^{-/-}, and CXCL1 rescued MC38-DCLK1^{-/-} tumors on the seventh day after implantation. (F) Four cell lines, MC38 DCLK1^{WT}, MC38 DCLK1^{-/-}, MC38 DCLK1^{-/-}-CXCL1^{OE}, and MC38 DCLK1^{-/-}-CXCL2^{OE} were inoculated with 1.5 × 10⁶ cells per mouse *in situ* in the intestine, and the tumor growth of each group was compared after the mice were killed on the 21st day after tumor inoculation (The arrowheads indicates the site of intestinal tumor formation). (G) Subcutaneous tumor growth in mice injected with MC38-DCLK1^{WT} and DCLK1^{-/-} cells treated daily with SB265610 (CXCR2 inhibitor, 2 mg/kg body weight) or PBS control starting from tumor inoculation. (H) Flow cytometry quantification of CD8⁺T cells and the MDSC percentage for subcutaneous tumors receiving treatment on the seventh day after implantation. (I) Mice were inoculated with MC38 DCLK1-WT and DCLK1-knockout (KO) colon cancer cell lines *in situ* and given CXCR2-receptor inhibitor SB265610 intraperitoneally for 14 days after 7 days of inoculation. After day 21, mice were killed and intestinal dissection was performed to compare tumor formation between the inhibitor-dosed and nondosed groups (The arrowheads indicates the site of intestinal tumor formation). Data are presented as means ± SD; n = 5–7 tumors for each group. *P < .05, **P < .01, ***P < .001, and ****P < .0001, 2-tailed Student t test. DMSO, dimethyl sulfoxide; ERKi, Extracellular signal-regulated kinase inhibitor; mRNA, messenger RNA; p-ERK, phosphorylate-Extracellular signal-regulated kinase inhibitor.

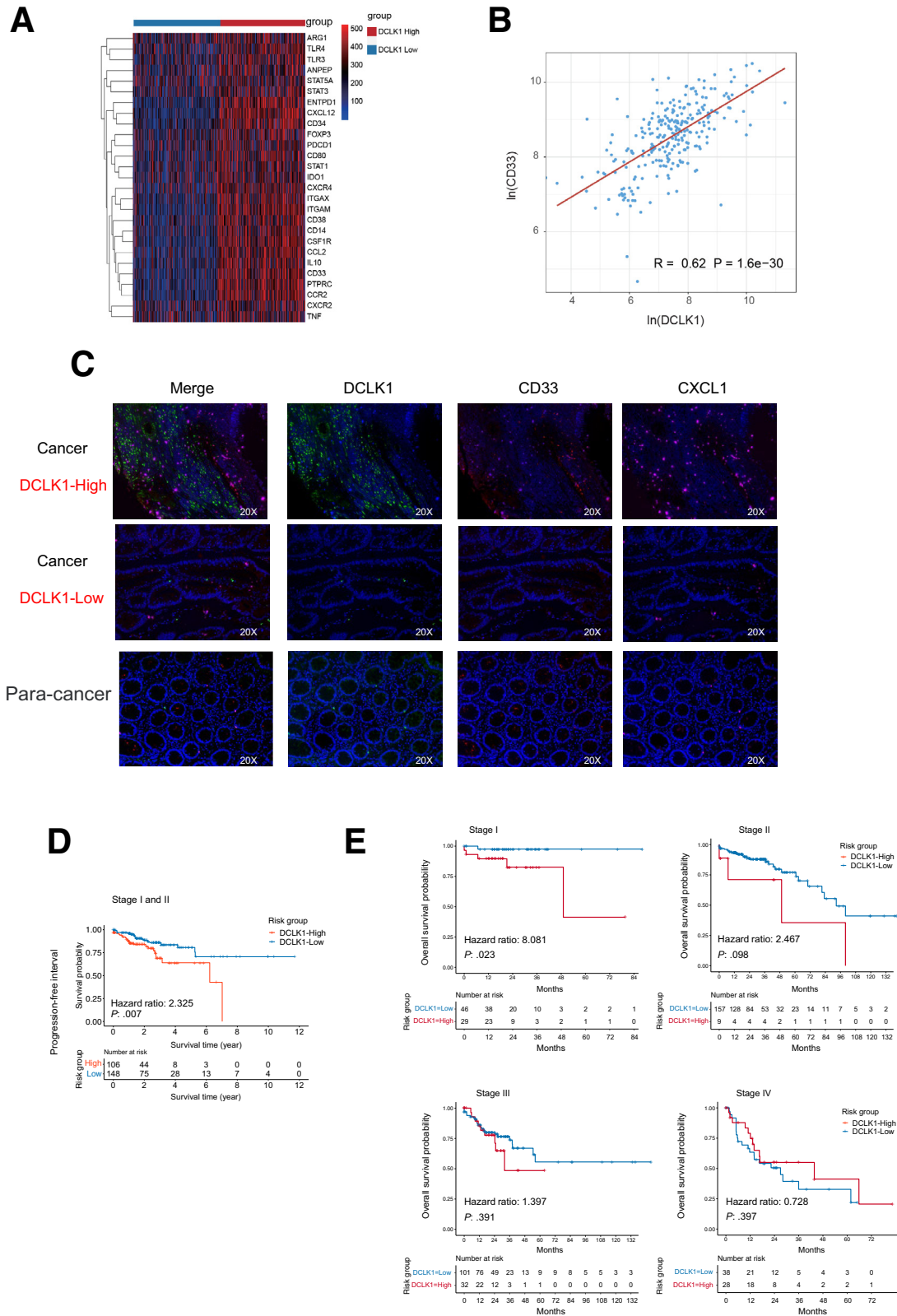


Figure 9. The expression of DCLK1 is associated with CXCL1 expression, MDSC infiltration, and poor prognosis in colon cancer patients. (A) Expression correlations between DCLK1 and known genes that actively are involved in MDSC regulation. The transcriptome profiling samples from patients with colon cancer (TCGA-COAD project) were used. (B) The correlation scatterplot shows a significant correlation between the expression of DCLK1 and CD33. The same batch of profiling samples as in panel A was used. Expression levels were log(ln)-transformed. (C) Fluorescence staining of CRC tissues shows that the expression and release of CD33 and CXCL1 in tumor tissues with high expression of DCLK1 are significantly higher than those in adjacent and low DCLK1 expression tissues. (D) Expression levels of DCLK1 have a notable impact on disease progression-free survival in patients with stage I/II (according to tumor node metastasis -TNM classification of tumor). (E) Expression levels of DCLK1 have a notable impact on overall survival of stage I patients.

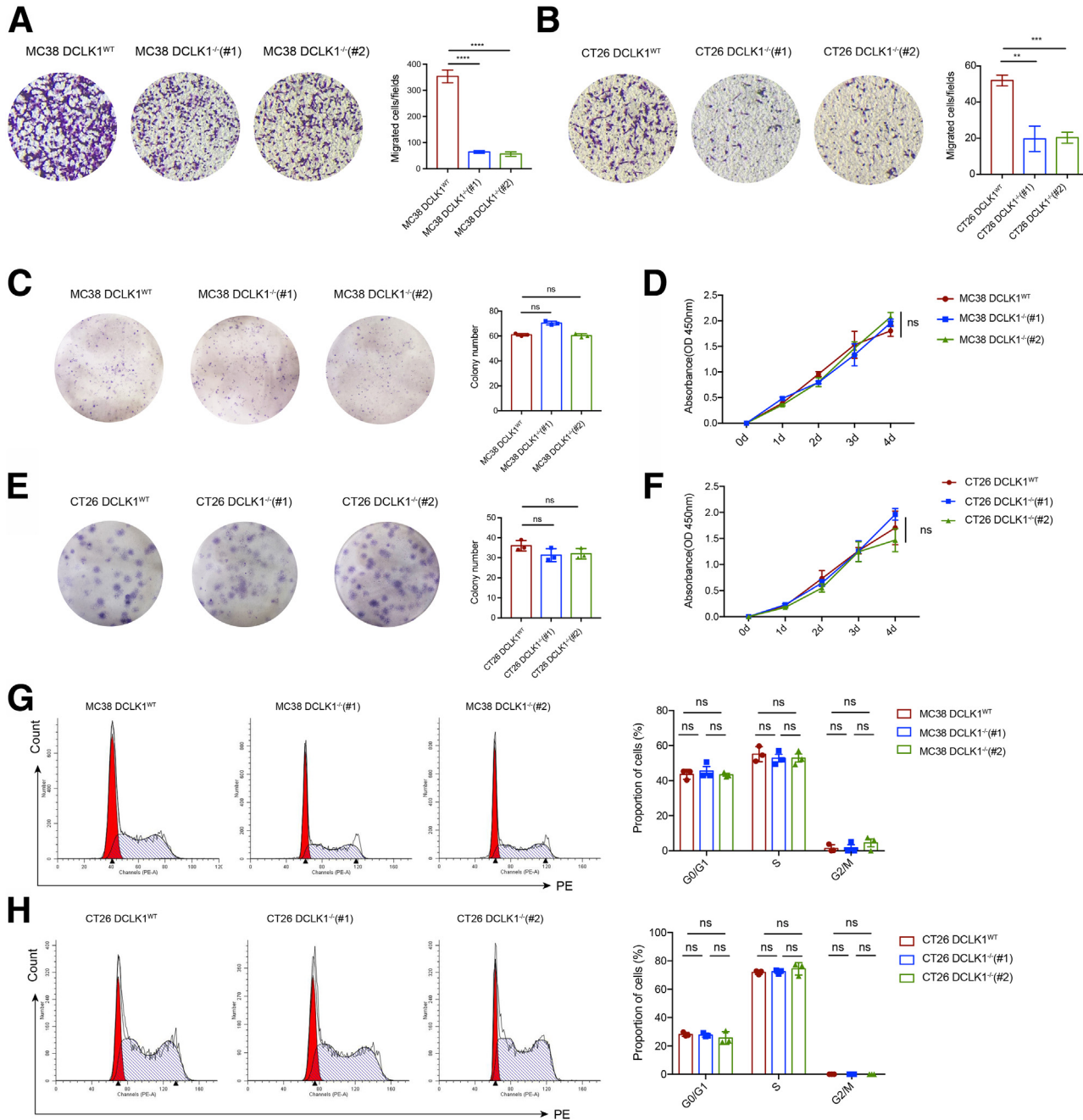


Figure 10. DCLK1 deletion reduces the migration ability of tumor cells, but not proliferation, *in vitro*. (A and B) The cell migration ability of DCLK1^{WT} and DCLK1^{-/-} cells was analyzed by Transwell assays. Significantly reduced cell migration was detected after down-regulation of DCLK1 in both MC38 and CT26 cells. (C–F) The deletion of DCLK1 did not affect tumor proliferation of MC38 and CT26 cell lines *in vitro*. (C and E) Representative images of the colony-formation assay are shown. (D and F) The Cell Counting Kit-8 (CCK-8) experiments show the growth curve of the MC38 and CT26 cell lines. (G and H) The cell cycle of MC38-DCLK1^{WT}, MC38-DCLK1^{-/-} and CT26-DCLK1^{WT}, CT26-DCLK1^{-/-} were analyzed by flow cytometry. *Right*: Representative images of cell-cycle assays. *left*: The percentage of each phase is shown. Data are presented as means \pm SD, ** $P < .01$, *** $P < .001$, and **** $P < .0001$, 2-tailed Student *t* test.

targeting DCLK1 may be a promising target for immunotherapy in CRC. Our work sheds light on how DCLK1 contributes to CRC immune evasion by allowing tumor cells to escape from immunosurveillance. Furthermore, our results provide a rationale to develop CXCR2 antagonists and DCLK1 inhibitors as therapeutic approaches to subverting tumor-induced immunosuppression. For early colon cancer

patients with high DCLK1 expression, we may be able to combine DCLK1 inhibitors (such as LRRK2-IN-1, XMD8-92, and DCLK1-IN-1) or CXCR2 inhibitors (navarixin) with existing antineoplastic treatment to overcome immune tolerance and prolong progression-free survival. In addition, DCLK1 may serve as a biomarker to predict the survival of patients and provide guidance for clinical treatment.

Materials and Methods

Cell Lines

The MC38, CT26, SW480, and HCT116 CRC cell lines and 293FT cells were obtained from American Type Culture Collection (Manassas, VA). MC38 and CT26 cells were cultured with RPMI1640 (Gibco, Shanghai, China), SW480 cells were cultured in L-15 medium, HCT116 cells were cultured in McCoy's 5A medium, and 293FT cells were cultured in high-glucose Dulbecco's modified Eagle medium (Gibco, Shanghai, China). All medium was supplemented with fetal bovine serum (FBS) (10%; Albany, Australia), penicillin (100 U/mL), and streptomycin (100 mg/mL). The incubator maintained an atmosphere of 5% CO₂ at 37°C for the MC38, CT26, HCT116, and 293FT cell lines. For the SW480 cell line, CO₂-free culture conditions were used as recommended by American Type Culture Collection.

Gene Deletion of DCLK1 by the CRISPR/Cas9 System

DCLK1-deficient cells were constructed through CRISPR/Cas9 technology. According to the principle of the CRISPR/Cas9 system, we designed the single-guide RNA to target the DCLK1 gene. The sequences used for mouse DCLK1 are as follows: 5'-GCATTTTGTGATGAGCGGGACA-3' and 5'-AGCAGGGGGTCCCGTGTGAA-3', and for human DCLK1 is 5'-CACCGGAGTAGAGAGCTGACTACCA-3'. The single-guide RNA sequences were ligated with linearized LentiCRISPR V2 plasmids. Two plasmids, psPAX2 and pMD2.G, were used for packaging plasmid. We co-transfected the 3 plasmids in 293FT cells for Lentivirus packaging and then collected the supernatant to harvest lentivirus to infect the MC38, CT26, and SW480 cells. After the infection, all 3 cell lines were selected with puromycin.

DCLK1 Overexpression

DCLK1 overexpression was achieved by transient transfection of the pLVX-IRES-DCLK1-ZsGreen 1 plasmid into the HCT116 cell line using Neofect (Biotech Co, Ltd, Beijing, China) according to the manufacturer's instructions. The empty vector was used as a negative control.

Subcutaneous Tumor Growth

C57BL/6J, BALB/c, and nude mice were obtained from Charles River Laboratory (Beijing, China). In all experiments, 6- to 8-week-old mice were used. All mice were kept in a barrier facility at the animal center of Tsinghua University (Beijing, China). The animal facility in the laboratory has been licensed by the Association for Assessment and Accreditation of Laboratory Animal Care International. For the xenograft tumor model, 1×10^6 tumor cells were implanted SC into the right flanks of mice with 3 different genetic backgrounds. Tumor volume was measured every 4–5 days. The following formula was used to calculate the tumor volumes: $V (\text{mm}^3) = (\text{length} \times \text{width}^2)/2$. All animal experiments in this study were approved by the animal ethics committee.

Establishment of Intestinal Carcinoma In Situ

The tumor cells were adjusted to $3 \times 10^7/\text{mL}$ and mixed with an equal volume of melted Matrigel (BD Biosciences, Heidelberg, Germany) at a final concentration of 1.5×10^6 cells per 100 μL . Mice received 5% chloral hydrate intraperitoneally for anesthesia. The injection volume corresponded to mouse weight, that is, 200 μL chloral hydrate per 20-gram mouse. After anesthesia, we maintained the mice at a 37°C constant-temperature operating table in an abdominal-upward position. An opening was made in the left lower abdomen of the mice to expose the colon, and 100 μL cell suspension coated with Matrigel (1.5×10^6 cells) was injected into the intestinal wall. After the injection, the abdominal incision was closed using a wound suture clamp. The anesthetized mice awakened 2 hours later, and their vital signs were observed daily. Three weeks later, the mice were killed and dissected to check the tumor growth.

Tumor Growth After Rechallenge

DCLK1^{-/-} MC38 cells (1×10^6) were implanted SC into the left flank of C57BL/6J mice and DCLK1^{-/-} CT26 cells were implanted in BALB/c mice. Tumor volumes were measured by caliper every 4–5 days. After the DCLK1^{-/-} tumors regressed, DCLK1^{WT} or DCLK1^{-/-} tumor cells were implanted into the right abdomen of mice SC, and marked as the experimental group. We continued to observe the growth of tumor cells in the 2 groups. In the control group, the mice were implanted with only DCLK1^{WT} or DCLK1^{-/-} cells SC at 28 days, without any prior inoculation.

CD4⁺, CD8⁺ T-Cell Depletion

In vivo T-cell depletion was performed through intraperitoneal injection. Anti-CD4, anti-CD8 (clone GK1.5 and clone 53-6.7, respectively), and isotype control antibody were purchased from eBioscience, San Diego, CA. Before the SC injection of tumor cells, mice were injected with 150 μg antibody 4 times. After the mice were inoculated with tumor cells, the antibody was injected intraperitoneally at 3-day intervals to completely deplete the T cells. On day 8 after the initial antibody injection, each group, containing 6–8 mice, was inoculated with 1×10^6 MC38 DCLK1^{WT} and DCLK1^{-/-} cells SC.

Flow Cytometry Analysis of Immune Cell Populations

For flow cytometry analysis, the tumor-bearing mice were killed by CO₂ asphyxiation and the tumor tissues were removed on the seventh day after tumor inoculation. The tumor tissues were digested with Dulbecco's modified Eagle medium/RPMI 1640 medium containing 2 mg/mL collagenase IV for 0.5 hours at 37°C. Next, the tumor tissues were dissociated by gentleMACS Tissue Dissociator (Miltenyi Biotec, Bergisch Gladbach, Germany) and run through a 70- μm cell strainer to obtain a single-cell suspension. Samples were centrifuged at 1000 rpm for 5 minutes twice and resuspended in fluorescence-activated cell sorter buffer. To stain intracellularly, we permeabilized the cell membrane with Foxp3/transcription factor staining buffer. All antibodies for flow cytometry population analysis are listed in

Tables 1–3. Nonviable cells were stained with the LIVE/DEAD Fixable Aqua Dead Cell Stain Kit (Thermo Fisher Scientific, Waltham, MA) and gated out. Experiments were performed using a BD Biosciences FACS Aria III, and results were analyzed using FlowJo software (Palo Alto, CA).

CD8+ T-Cell Fluorescent Immunohistochemistry

Seven days after the mice were inoculated, tumor-bearing mice were killed and tumor tissues were taken. All tissues were embedded in Optimal Cutting Temperature (OCT) cryostat sectioning medium and stored at -80°C . Before sectioning, tissue blocks were kept at -20°C overnight. Frozen blocks were sectioned onto 5- μm -thick slides and kept in 1% paraformaldehyde at room temperature for approximately 3 minutes. After permeabilization with 0.5% Triton-X 100 (Beyotime, Beijing, China) for 30 minutes, antigen retrieval was performed with glycine. Before staining, all slides were blocked for 1 hour at room temperature with 0.2% Tween-20 and 5% FBS to avoid nonspecific binding. Staining with primary antibodies was performed at 4°C in moist dark chambers overnight. Primary antibodies were diluted in antibody diluent ($1 \times$ phosphate-buffered saline [PBS] + 0.2% Tween-20 + 5% FBS + 0.05% NaN_3). The anti-mouse CD8 α (clone 53-6.7) antibody was diluted at 1:100, rat IgG2a was used as a negative control (eBioscience, San Diego, CA) and diluted at 1:100. After staining with primary antibodies, we washed the slides with PBS for 10 minutes. Slides were incubated with secondary antibodies for more than 2 hours in a moist dark chamber at a dilution of 1:1000 (Alexa Fluor 488-AffiniPure goat anti-rabbit IgG; H+L) (Jackson ImmunoResearch, West Grove, PA). After removal of secondary antibodies, the slides were mounted with a mounting medium containing 4',6-diamidino-2-phenylindole (100 ng/mL). After washing, slides were sealed with a coverslip and observed with LSCM-FV1200 laser scanning confocal microscopy (Olympus, Tokyo, Japan). Three tumor sections were stained in each group.

RNA Sequence Analysis

Gene expression profiling. RNA-seq libraries were sequenced on a BGISEQ-500 (BGI, Shenzhen, China). The yielded reads then were aligned to mm10 reference genome using STAR 2.6.0a,⁶⁴ with the following parameters as `-outFilterMultimapNmax 20 -alignSJDBoverhangMin 1 -outFilterMismatchNmax 999 -outFilterMismatchNoverReadLmax 0.04 -alignIntronMin 20 -alignIntronMax 1000000 -outFilterIntronMotifs RemoveNoncanonicalUnannotated -sjdbScore 1 -sjdbOverhang 49 -quantMode GeneCounts`. Aligned reads were quantified by STAR using GENCODE M20 as reference. The data and analysis pipeline were managed by BioQueue.⁶⁵ To identify differentially expressed genes, we used edgeR,⁶⁶ which also provided us depth-normalized read counts. Another R package, pheatmap, was used to visualize expression profiles.

Enrichment Analysis

We further performed both GO and KEGG enrichment analysis on these identified differentially expressed genes using cluster Profile.⁶⁷ For GO enrichment, we considered as

Table 1. T-Cell Subsets for Flow Cytometry Analysis to Define Immune Cell Populations

Population	Markers
CD4+ T cells	CD45+CD3+CD4+CD8-
CD4+ effector T cells	CD45+CD3+CD4+CD8-CD44+CD62L-
CD8+ T cells	CD45+CD3+CD4-CD8+
CD8+ effector T cells	CD45+CD3+CD4-CD8+CD44+CD62L-
Markers	Fluorophore
Viability	Auqa
CD45	APC-eFluor780
CD3	APC
CD4	BV605
CD8	BV421
CD44	FITC
CD62L	PE

APC, Allophycocyanin; FITC, fluorescein isothiocyanate; PE, Phycoerythrin.

significant the ontology terms with q values smaller than 0.05 adjusted by Benjamini and Hochberg (BH). For KEGG enrichment, we required significant pathways to have *P* values less than .05.

Association Analysis

Association analysis between DCLK1 and the MAPK-ERK pathway was performed with cor.test from R. Functional protein association networks between DCLK1 and proteins in the MAPK-ERK pathway was predicted by STRING (version 11),⁶⁸ using an interaction score of 0.400 as a cut-off value. To validate our conclusion in human beings, we retrieved Fragments Per Kilobase of exon model per Million mapped fragments (FPKM) values of homogeneous genes from the TCGA-COAD project ($n = 480$) and calculated their correlation coefficients.

Survival Analysis

All of the messenger RNA expression data for TCGA data set analysis were downloaded from UCSC Xena (<https://xenabrowser.net/datapages>) (University of California, Santa Cruz) in FPKM format. Samples with incomplete information or survival time shorter than 30 days were excluded and the optimal cut-off point of risk value was performed using the surv_cutpoint function in R package survminer to avoid bias.

Mouse MDSCs (CD11b+Gr1+) Isolation and Co-culture With T Cells

Subcutaneous DCLK1^{WT} and DCLK1^{-/-} tumors were dissected, digested with collagenase IV (Worthington) at 37°C , and filtered to a single-cell suspension. The EasySep Mouse MDSC (CD11b+ Gr1+) Isolation Kit (Stemcell, Vancouver, Canada) was used to isolate MDSCs from tumor tissues. The purity of MDSCs, as indicated by flow cytometry, was greater than 70%. The corresponding spleens of

Table 2. MDSC Subsets for Flow Cytometry Analysis to Define Immune Cell Populations

Population	Markers
Macrophage	CD45+CD11b+F4/80+
G-MDSC	CD45+CD11b+F4/80-Gr1+Ly6G+
M-MDSC	CD45+CD11b+F4/80-Gr1+Ly6C+
Markers	Fluorophore
Viability	Aqua
CD45	APC-eFluor780
CD11b	AF700
F4/80	PE
Gr1	AF594
Ly6G	BV421
Ly6C	FITC

APC, Allophycocyanin; FITC, fluorescein isothiocyanate; M-MDSC, monocytic myeloid-derived suppressor cell; PE, Phycoerythrin.

DCLK1^{WT} and DCLK1^{-/-} groups were isolated, and the EasySep Mouse CD8+ T-Cell Isolation Kit (Stemcell, Vancouver, Canada) was used to extract CD8+ T cells from the spleen of mice and stained with CFSE (10 μ mol/L). The sorted MDSCs were co-cultured with CFSE-labeled T cells at a 1:1 ratio, and mouse CD3/CD28 (eBioscience, San Diego, CA) was added to activate the T cells. After 3 days, the proliferation of T cells was detected by flow cytometry.

Multiplexed Immunofluorescence

A colon cancer tissue microarray (HCol-Ade060CS1-01) containing 30 paired tissues of stage I/II intestinal cancer and matched paracancerous tissues was purchased from Core Ultra (Shanghai, China). This tissue microarray was stained with the Opal 4 Multiplex reagents (PerkinElmer, Waltham MA) containing DCLK1 (ab31704, 1:500) opal 690, CXCL1 (ab89318, 1:500) opal 570, and CD33 (ab269456, 1:500) opal 590, and then counterstained with 4',6-diamidino-2-phenylindole. Multiplexed fluorophore-stained slides were photographed under an Olympus confocal

Table 3. NK and NKT Cells for Flow Cytometry Analysis to Define Immune Cell Populations

Population	Markers
NK	CD45+CD3-NK1.1+
NKT	CD45+CD3+NK1.1+
Markers	Fluorophore
Viability	Aqua
CD45	APC-eFluor780
CD3	APC
NK1.1	FITC

APC, Allophycocyanin; FITC, fluorescein isothiocyanate; NKT, Natural killer T.

microscope (Tokyo, Japan). The background was removed using plain white film and finally analyzed using the inForm software (Beijing, China).

Western Blot Analysis

DCLK1^{WT} and DCLK1^{-/-} tumor cells (1×10^6) were seeded in 60-mm dishes and cultured for 24 hours. Protease and phosphatase inhibitors (Beyotime, Beijing, China) were dissolved in RIPA buffer. After the cells adhered, the culture supernatant was removed and the RIPA buffer was added for cell lysis. Cells were lysed with RIPA buffer on ice for half an hour. Total protein was extracted and concentrations were measured by BCA protein assay (Thermo Fisher Scientific, Waltham, MA). The Nuclear Extraction Kit (Beyotime, Beijing, China) was used for cytoplasmic and nuclear protein isolation. The protein samples were applied to 8%–12% sodium dodecyl sulfate–polyacrylamide gel electrophoresis and transferred onto a polyvinylidene difluoride membrane (Millipore Corporation, Billerica, MA). After 8% nonfat milk blockade for 1 hour, the membrane was incubated with primary antibodies at 4°C overnight. Primary antibodies included anti-DCLK1 (1:1000, cat# 62257; Cell Signaling Technology and cat# 31704; Abcam, Cambridge, UK), anti-ERK1/2 (1:1000, cat# 4695; Cell Signaling Technology), anti-phospho-ERK (1:1000, cat# 9101; Cell Signaling Technology), c-Myc (1:1000, CST#18583; Cell Signaling Technology), lamin A/C (1:1000, cat# 4777; Cell Signaling Technology), and anti-glyceraldehyde-3-phosphate dehydrogenase (GAPDH) (1:1000, cat# 5174; Cell Signaling Technology). After the polyvinylidene difluoride membrane was washed 3 times by $1 \times$ Tris-buffered saline with Tween-20, the secondary antibodies were incubated for 1 hour at room temperature. The membrane was developed with the imaging system (Bio-Rad, Irvine, CA).

RNA Extraction and Quantitative Real-Time PCR

Total RNA was extracted using TRIzol reagent (Invitrogen, Carlsbad, CA). To prepare complementary DNA using the PrimeScript RT reagent Kit (RR047A; TaKaRa, Beijing, China), 1 μ g total RNA was reverse-transcribed. Expression of specific genes was verified using the SYBR Green system (Applied Biosystems, Waltham, MA), normalized with GAPDH. In the RT-PCR system, all PCR reactions contained forward and reverse primers (100 pmol). The RT-PCR reaction was performed on a 7500 Sequence Detection System (Applied Biosystems, Waltham, MA). With the comparative Cycle Threshold (Ct) method, we measured the relative gene expression changes ($X = 2^{-\Delta\Delta Ct}$). Sequences of quantitative PCR primers are listed as follows: CXCL1 of mice: 5'-CTGGGATTCACCTCAAGAATC-3' and 5'-CAGGGTCAAGGCAAGCCTC-3'; CXCL1 of human beings: 5'-TCCTGCATCCCCATAGTTA-3' and 5'-CTTCAGGAA-CAGCCACCAGT-3'; CXCL2 of mice: 5'-CCAACCACCAGGTA-CAGG-3' and 5'-GCGTCACACTCAAGCTCTG-3'; CXCL2 of human beings: 5'-CCCATGGTTAAGAAAATCATCG-3' and 5'-CTTCAGGAA-CAGCCACCAAT-3'; GAPDH of mice: 5'-ATCAA-GAAGGTGGTGAAGCA-3' and 5'-AGACAACCTGGTCTCAGTGT-

3'; GAPDH of human beings: 5'-ACAACTTTGGTATCGTG-GAAGG-3' and 5'-GCCATCACGCCACAGTTTC-3'.

ELISA Assays

The tumor cells were seeded evenly on a 6-well plate for 24 hours. After that, cell culture supernatant was collected. To remove cell fragments, the supernatant was centrifuged at $16,000 \times g$ for 10 minutes. The mouse CXCL1 and CXCL2 expression levels were measured by mouse Quantikine ELISA kits (MKC00B/MM200; R&D Systems), and the human CXCL1 and CXCL2 expression levels were measured by the Human SimpleStep ELISA Kit (ab190805/ab184862; Abcam). All of the experimental methods were performed according to the manufacturer's protocols.

Cell Proliferation and Migration Assays

The cell proliferation experiments were performed with the Cell Counting Kit-8 kit (Dojindo, Kumamoto-ken, Japan). The DCLK1^{WT} and DCLK1^{-/-} cells were seeded on a 96-well plate, and the absorbance was measured at 450-nm wavelength by a microplate reader for 4–5 days. Then, the proliferation curve was calculated.

Cells were seeded in the upper chamber of a 24-well, 8.0- μ m pore membrane chamber (Corning, Inc, Corning, NY) with FBS-free medium (1×10^5 cells for MC38 and 5×10^4 for CT26), followed by the addition of 600 μ L medium containing 10% FBS into the lower chamber. The MC38 and CT26 cells were cultured for 24 hours for migration. After 24 hours, we removed the nonmigrating cells from the upper chamber and fixed the chamber membranes with 4% Paraformaldehyde (PFA) for 10 minutes. The migrating cells were stained with crystal violet (0.1%) for 5 minutes, and stained cells were counted under the microscope.

Colony Formation Assays

MC38 and CT26 cells (2×10^2 /well) were seeded in 6-well plates, and the clone formation was detected under the microscope approximately 2–3 days. Two weeks later, we removed the culture media and washed with PBS twice, and then fixed with 4% PFA for 10 minutes, stained with crystal violet. Each clone contained more than 50 cells.

Statistical Analysis

All of the data are presented as means \pm SD. Two groups were compared using the Student *t* test. Data were analyzed with GraphPad Prism (version 9.0) (Software, San Diego, CA), and a *P* value $< .05$ was considered significant. Each independent experiment was repeated more than 3 times.

References

1. Siegel RL, Miller KD, Jemal A. Cancer statistics, 2020. *CA Cancer J Clin* 2020;70:7–30.
2. Stein U, Schlag PM. Clinical, biological, and molecular aspects of metastasis in colorectal cancer. *Recent Results Cancer Res* 2007;176:61–80.
3. Scalfani F. PD-1 inhibition in metastatic dMMR/MSI-H colorectal cancer. *Lancet Oncol* 2017;18:1141–1142.
4. Goldstein J, Tran B, Ensor J, Gibbs P, Wong HL, Wong SF, Vilar E, Tie J, Broaddus R, Kopetz S, Desai J, Overman MJ. Multicenter retrospective analysis of metastatic colorectal cancer (CRC) with high-level microsatellite instability (MSI-H). *Ann Oncol* 2014;25:1032–1038.
5. Zeuner A, Todaro M, Stassi G, De Maria R. Colorectal cancer stem cells: from the crypt to the clinic. *Cell Stem Cell* 2014;15:692–705.
6. Plaks V, Kong N, Werb Z. The cancer stem cell niche: how essential is the niche in regulating stemness of tumor cells? *Cell Stem Cell* 2015;16:225–238.
7. Oskarsson T, Batlle E, Massagué J. Metastatic stem cells: sources, niches, and vital pathways. *Cell Stem Cell* 2014;14:306–321.
8. Ye J, Wu D, Wu P, Chen Z, Huang J. The cancer stem cell niche: cross talk between cancer stem cells and their microenvironment. *Tumour Biol* 2014;35:3945–3951.
9. Prager BC, Xie Q, Bao S, Rich JN. Cancer stem cells: the architects of the tumor ecosystem. *Cell Stem Cell* 2019;24:41–53.
10. Chandrakesan P, Panneerselvam J, Qu D, Weygant N, May R, Bronze MS, Houchen CW. Regulatory roles of Dclk1 in epithelial mesenchymal transition and cancer stem cells. *J Carcinog Mutagen* 2016;7:257.
11. Nakanishi Y, Seno H, Fukuoka A, Ueo T, Yamaga Y, Maruno T, Nakanishi N, Kanda K, Komekado H, Kawada M, Isomura A, Kawada K, Sakai Y, Yanagita M, Kageyama R, Kawaguchi Y, Taketo MM, Yonehara S, Chiba T. Dclk1 distinguishes between tumor and normal stem cells in the intestine. *Nat Genet* 2013;45:98–103.
12. May R, Riehl TE, Hunt C, Sureban SM, Anant S, Houchen CW. Identification of a novel putative gastrointestinal stem cell and adenoma stem cell marker, doublecortin and CaM kinase-like-1, following radiation injury and in adenomatous polyposis coli/multiple intestinal neoplasia mice. *Stem Cells* 2008;26:630–637.
13. Chandrakesan P, Yao J, Qu D, May R, Weygant N, Ge Y, Ali N, Sureban SM, Gude M, Vega K, Bannerman-Menson E, Xia L, Bronze M, An G, Houchen CW. Dclk1, a tumor stem cell marker, regulates pro-survival signaling and self-renewal of intestinal tumor cells. *Mol Cancer* 2017;16:30.
14. Weygant N, Qu D, Berry WL, May R, Chandrakesan P, Owen DB, Sureban SM, Ali N, Janknecht R, Houchen CW. Small molecule kinase inhibitor LRRK2-IN-1 demonstrates potent activity against colorectal and pancreatic cancer through inhibition of doublecortin-like kinase 1. *Mol Cancer* 2014;13:103.
15. Liu W, Wang S, Sun Q, Yang Z, Liu M, Tang H. DCLK1 promotes epithelial-mesenchymal transition via the PI3K/Akt/NF-kappaB pathway in colorectal cancer. *Int J Cancer* 2018;142:2068–2079.
16. Weygant N, Ge Y, Qu D, Kaddis JS, Berry WL, May R, Chandrakesan P, Bannerman-Menson E, Vega KJ, Tomasek JJ, Bronze MS, An G, Houchen CW. Survival of patients with gastrointestinal cancers can be predicted by a surrogate microRNA signature for cancer stem-like

- cells marked by DCLK1 kinase. *Cancer Res* 2016; 76:4090–4099.
17. Makino S, Takahashi H, Okuzaki D, Miyoshi N, Haraguchi N, Hata T, Matsuda C, Yamamoto H, Mizushima T, Mori M, Doki Y. DCLK1 integrates induction of TRIB3, EMT, drug resistance and poor prognosis in colorectal cancer. *Carcinogenesis* 2020;41:303–312.
 18. Zhang Y, Zoltan M, Riquelme E, Xu H, Sahin I, Castro-Pando S, Montiel MF, Chang K, Jiang Z, Ling J, Gupta S, Horne W, Pruski M, Wang H, Sun SC, Lozano G, Chiao P, Maitra A, Leach SD, Kolls JK, Vilar E, Wang TC, Bailey JM, McAllister F. Immune cell production of interleukin 17 induces stem cell features of pancreatic intraepithelial neoplasia cells. *Gastroenterology* 2018; 155:210–223 e3.
 19. Qu D, Weygant N, May R, Chandrakesan P, Madhoun M, Ali N, Sureban SM, An G, Schlosser MJ, Houchen CW. Ablation of doublecortin-like kinase 1 in the colonic epithelium exacerbates dextran sulfate sodium-induced colitis. *PLoS One* 2015;10:e0134212.
 20. Sureban SM, Berahovich R, Zhou H, Xu S, Wu L, Ding K, May R, Qu D, Bannerman-Menson E, Golubovskaya V, Houchen CW. DCLK1 monoclonal antibody-based CAR-T cells as a novel treatment strategy against human colorectal cancers. *Cancers (Basel)* 2019;12:54.
 21. Gabrilovich DI, Nagaraj S. Myeloid-derived suppressor cells as regulators of the immune system. *Nat Rev Immunol* 2009;9:162–174.
 22. Marvel D, Gabrilovich DI. Myeloid-derived suppressor cells in the tumor microenvironment: expect the unexpected. *J Clin Invest* 2015;125:3356–3364.
 23. Kumar V, Patel S, Tcyganov E, Gabrilovich DI. The nature of myeloid-derived suppressor cells in the tumor microenvironment. *Trends Immunol* 2016;37:208–220.
 24. Wesolowski R, Markowitz J, Carson WE 3rd. Myeloid derived suppressor cells - a new therapeutic target in the treatment of cancer. *J Immunother Cancer* 2013;1:10.
 25. Youn JI, Nagaraj S, Collazo M, Gabrilovich DI. Subsets of myeloid-derived suppressor cells in tumor-bearing mice. *J Immunol* 2008;181:5791–5802.
 26. Gabrilovich DI, Ostrand-Rosenberg S, Bronte V. Coordinated regulation of myeloid cells by tumours. *Nat Rev Immunol* 2012;12:253–268.
 27. Kato H, Wang D, Daikoku T, Sun H, Dey SK, Dubois RN. CXCR2-expressing myeloid-derived suppressor cells are essential to promote colitis-associated tumorigenesis. *Cancer Cell* 2013;24:631–644.
 28. Gao D, Joshi N, Choi H, Ryu S, Hahn M, Catena R, Sadik H, Argani P, Wagner P, Vahdat LT, Port JL, Stiles B, Sukumar S, Altorki NK, Raffi S, Mittal V. Myeloid progenitor cells in the premetastatic lung promote metastases by inducing mesenchymal to epithelial transition. *Cancer Res* 2012;72:1384–1394.
 29. Diaz-Montero CM, Salem ML, Nishimura MI, Garrett-Mayer E, Cole DJ, Montero AJ. Increased circulating myeloid-derived suppressor cells correlate with clinical cancer stage, metastatic tumor burden, and doxorubicin-cyclophosphamide chemotherapy. *Cancer Immunol Immunother* 2009;58:49–59.
 30. Gabbitass RF, Annels NE, Stocken DD, Pandha HA, Middleton GW. Elevated myeloid-derived suppressor cells in pancreatic, esophageal and gastric cancer are an independent prognostic factor and are associated with significant elevation of the Th2 cytokine interleukin-13. *Cancer Immunol Immunother* 2011;60:1419–1430.
 31. Duffy A, Zhao F, Haile L, Gamrekashvili J, Fioravanti S, Ma C, Kapanadze T, Compton K, Figg WD, Greten TF. Comparative analysis of monocytic and granulocytic myeloid-derived suppressor cell subsets in patients with gastrointestinal malignancies. *Cancer Immunol Immunother* 2013;62:299–307.
 32. Sun HL, Zhou X, Xue YF, Wang K, Shen YF, Mao JJ, Guo HF, Miao ZN. Increased frequency and clinical significance of myeloid-derived suppressor cells in human colorectal carcinoma. *World J Gastroenterol* 2012; 18:3303–3309.
 33. Zhang B, Wang Z, Wu L, Zhang M, Li W, Ding J, Zhu J, Wei H, Zhao K. Circulating and tumor-infiltrating myeloid-derived suppressor cells in patients with colorectal carcinoma. *PLoS One* 2013;8:e57114.
 34. Serrels A, Lund T, Serrels B, Byron A, McPherson RC, von Kriegsheim A, Gomez-Cuadrado L, Canel M, Muir M, Ring JE, Maniati E, Sims AH, Pachter JA, Brunton VG, Gilbert N, Anderton SM, Nibbs RJ, Frame MC. Nuclear FAK controls chemokine transcription, Tregs, and evasion of anti-tumor immunity. *Cell* 2015;163:160–173.
 35. Di Mitri D, Toso A, Alimonti A. Molecular pathways: targeting tumor-infiltrating myeloid-derived suppressor cells for cancer therapy. *Clin Cancer Res* 2015; 21:3108–3112.
 36. Veglia F, Perego M, Gabrilovich D. Myeloid-derived suppressor cells coming of age. *Nat Immunol* 2018; 19:108–119.
 37. Gabrilovich DI. Myeloid-derived suppressor cells. *Cancer Immunol Res* 2017;5:3–8.
 38. Wang D, Sun H, Wei J, Cen B, DuBois RN. CXCL1 is critical for premetastatic niche formation and metastasis in colorectal cancer. *Cancer Res* 2017;77:3655–3665.
 39. Chaikwad A, Tacconi EM, Zimmer J, Liang Y, Gray NS, Tarsounas M, Knapp S. A unique inhibitor binding site in ERK1/2 is associated with slow binding kinetics. *Nat Chem Biol* 2014;10:853–860.
 40. Marampon F, Ciccarelli C, Zani BM. Down-regulation of c-Myc following MEK/ERK inhibition halts the expression of malignant phenotype in rhabdomyosarcoma and in non muscle-derived human tumors. *Mol Cancer* 2006; 5:31.
 41. Tsai WB, Aiba I, Long Y, Lin HK, Feun L, Savaraj N, Kuo MT. Activation of Ras/PI3K/ERK pathway induces c-Myc stabilization to upregulate argininosuccinate synthetase, leading to arginine deiminase resistance in melanoma cells. *Cancer Res* 2012;72:2622–2633.
 42. Yang G, Rosen DG, Liu G, Yang F, Guo X, Xiao X, Xue F, Mercado-Urbe I, Huang J, Lin SH, Mills GB, Liu J. CXCR2 promotes ovarian cancer growth through dysregulated cell cycle, diminished apoptosis, and enhanced angiogenesis. *Clin Cancer Res* 2010; 16:3875–3886.

43. Singh S, Varney M, Singh RK. Host CXCR2-dependent regulation of melanoma growth, angiogenesis, and experimental lung metastasis. *Cancer Res* 2009; 69:411–415.
44. Ning Y, Labonte MJ, Zhang W, Bohanes PO, Gerger A, Yang D, Benhaim L, Paez D, Rosenberg DO, Nagulapalli Venkata KC, Louie SG, Petasis NA, Ladner RD, Lenz HJ. The CXCR2 antagonist, SCH-527123, shows antitumor activity and sensitizes cells to oxaliplatin in preclinical colon cancer models. *Mol Cancer Ther* 2012; 11:1353–1364.
45. Liao W, Overman MJ, Boutin AT, Shang X, Zhao D, Dey P, Li J, Wang G, Lan Z, Li J, Tang M, Jiang S, Ma X, Chen P, Katkhuda R, Korphisam K, Chakravarti D, Chang A, Spring DJ, Chang Q, Zhang J, Maru DM, Maeda DY, Zebala JA, Kopetz S, Wang YA, DePinho RA. KRAS-IRF2 axis drives immune suppression and immune therapy resistance in colorectal cancer. *Cancer Cell* 2019;35:559–572 e7.
46. Gao T, Wang M, Xu L, Wen T, Liu J, An G. DCLK1 is up-regulated and associated with metastasis and prognosis in colorectal cancer. *J Cancer Res Clin Oncol* 2016; 142:2131–2140.
47. Westphalen CB, Takemoto Y, Tanaka T, Macchini M, Jiang Z, Renz BW, Chen X, Ormanns S, Nagar K, Taylor Y, May R, Cho Y, Asfaha S, Worthley DL, Hayakawa Y, Urbanska AM, Quante M, Reichert M, Broyde J, Subramaniam PS, Remotti H, Su GH, Rustgi AK, Friedman RA, Honig B, Califano A, Houchen CW, Olive KP, Wang TC. Dclk1 defines quiescent pancreatic progenitors that promote injury-induced regeneration and tumorigenesis. *Cell Stem Cell* 2016; 18:441–455.
48. Qu D, Weygant N, Yao J, Chandrakesan P, Berry WL, May R, Pitts K, Husain S, Lightfoot S, Li M, Wang TC, An G, Clendenin C, Stanger BZ, Houchen CW. Overexpression of DCLK1-AL increases tumor cell invasion, drug resistance, and KRAS activation and can be targeted to inhibit tumorigenesis in pancreatic cancer. *J Oncol* 2019;2019:6402925.
49. Ge Y, Weygant N, Qu D, May R, Berry WL, Yao J, Chandrakesan P, Zheng W, Zhao L, Zhao KL, Drake M, Vega KJ, Bronze MS, Tomasek JJ, An G, Houchen CW. Alternative splice variants of DCLK1 mark cancer stem cells, promote self-renewal and drug-resistance, and can be targeted to inhibit tumorigenesis in kidney cancer. *Int J Cancer* 2018;143:1162–1175.
50. Weygant N, Qu D, May R, Tierney RM, Berry WL, Zhao L, Agarwal S, Chandrakesan P, Chinthalapally HR, Murphy NT, Li JD, Sureban SM, Schlosser MJ, Tomasek JJ, Houchen CW. DCLK1 is a broadly dysregulated target against epithelial-mesenchymal transition, focal adhesion, and stemness in clear cell renal carcinoma. *Oncotarget* 2015;6:2193–2205.
51. Sureban SM, May R, Weygant N, Qu D, Chandrakesan P, Bannerman-Menson E, Ali N, Pantazis P, Westphalen CB, Wang TC, Houchen CW. XMD8-9 inhibits pancreatic tumor xenograft growth via a DCLK1-dependent mechanism. *Cancer Lett* 2014;351:151–161.
52. Wu X, Qu D, Weygant N, Peng J, Houchen CW. Cancer stem cell marker DCLK1 correlates with tumorigenic immune infiltrates in the colon and gastric adenocarcinoma microenvironments. *Cancers (Basel)* 2020; 12:274.
53. Chandrakesan P, Panneerselvam J, May R, Weygant N, Qu D, Berry WR, Pitts K, Stanger BZ, Rao CV, Bronze MS, Houchen CW. DCLK1-isoform2 alternative splice variant promotes pancreatic tumor immunosuppressive M2-macrophage polarization. *Mol Cancer Ther* 2020;19:1539–1549.
54. Cao Z, Weygant N, Chandrakesan P, Houchen CW, Peng J, Qu D. Tuft and cancer stem cell marker DCLK1: a new target to enhance anti-tumor immunity in the tumor microenvironment. *Cancers (Basel)* 2020; 12:3801.
55. Yan R, Li J, Zhou Y, Yao L, Sun R, Xu Y, Ge Y, An G. Inhibition of DCLK1 down-regulates PD-L1 expression through Hippo pathway in human pancreatic cancer. *Life Sci* 2020;241:117150.
56. Talmadge JE, Gabrilovich DI. History of myeloid-derived suppressor cells. *Nat Rev Cancer* 2013; 13:739–752.
57. Steele CW, Karim SA, Leach JDG, Bailey P, Upstill-Goddard R, Rishi L, Foth M, Bryson S, McDaid K, Wilson Z, Eberlein C, Candido JB, Clarke M, Nixon C, Connelly J, Jamieson N, Carter CR, Balkwill F, Chang DK, Evans TRJ, Strathdee D, Biankin AV, Nibbs RJB, Barry ST, Sansom OJ, Morton JP. CXCR2 inhibition profoundly suppresses metastases and augments immunotherapy in pancreatic ductal adenocarcinoma. *Cancer Cell* 2016;29:832–845.
58. Yang L, DeBusk LM, Fukuda K, Fingleton B, Green-Jarvis B, Shyr Y, Matrisian LM, Carbone DP, Lin PC. Expansion of myeloid immune suppressor Gr⁺CD11b⁺ cells in tumor-bearing host directly promotes tumor angiogenesis. *Cancer Cell* 2004; 6:409–421.
59. Le DT, Uram JN, Wang H, Bartlett BR, Kemberling H, Eyring AD, Skora AD, Luber BS, Azad NS, Laheru D, Biedrzycki B, Donehower RC, Zaheer A, Fisher GA, Crocenzi TS, Lee JJ, Duffy SM, Goldberg RM, de la Chapelle A, Koshiji M, Bhajee F, Huebner T, Hruban RH, Wood LD, Cuka N, Pardoll DM, Papadopoulos N, Kinzler KW, Zhou S, Cornish TC, Taube JM, Anders RA, Eshleman JR, Vogelstein B, Diaz LA Jr. PD-1 blockade in tumors with mismatch-repair deficiency. *N Engl J Med* 2015;372:2509–2520.
60. Chen DS, Mellman I. Elements of cancer immunity and the cancer-immune set point. *Nature* 2017;541:321–330.
61. Sharma P, Hu-Lieskovan S, Wargo JA, Ribas A. Primary, adaptive, and acquired resistance to cancer immunotherapy. *Cell* 2017;168:707–723.
62. Davis RJ, Moore EC, Clavijo PE, Friedman J, Cash H, Chen Z, Silvín C, Van Waes C, Allen C. Anti-PD-L1 efficacy can be enhanced by inhibition of myeloid-derived suppressor cells with a selective inhibitor of PI3Kdelta/gamma. *Cancer Res* 2017;77:2607–2619.
63. Weber R, Fleming V, Hu X, Nagibin V, Groth C, Altevogt P, Utikal J, Umansky V. Myeloid-derived suppressor cells hinder the anti-cancer activity of immune checkpoint inhibitors. *Front Immunol* 2018;9:1310.

64. Dobin A, Davis CA, Schlesinger F, Drenkow J, Zaleski C, Jha S, Batut P, Chaisson M, Gingeras TR. STAR: ultra-fast universal RNA-seq aligner. *Bioinformatics* 2013; 29:15–21.
65. Yao L, Wang H, Song Y, Sui G. BioQueue: a novel pipeline framework to accelerate bioinformatics analysis. *Bioinformatics* 2017;33:3286–3288.
66. Robinson MD, McCarthy DJ, Smyth GK. edgeR: a Bioconductor package for differential expression analysis of digital gene expression data. *Bioinformatics* 2010; 26:139–140.
67. Yu G, Wang LG, Han Y, He QY. clusterProfiler: an R package for comparing biological themes among gene clusters. *Omics* 2012;16:284–287.
68. Szklarczyk D, Gable AL, Lyon D, Junge A, Wyder S, Huerta-Cepas J, Simonovic M, Doncheva NT, Morris JH, Bork P, Jensen LJ, Mering CV. STRING v11: protein-protein association networks with increased coverage, supporting functional discovery in genome-wide experimental datasets. *Nucleic Acids Res* 2019; 47:D607–D613.

Received July 15, 2021. Accepted October 18, 2022.

Correspondence

Address correspondence to: Yang Ge, MD, Beijing Chao-Yang Hospital, Department of Oncology, Capital Medical University, Beijing, 100020 China. e-mail: interna-1@163.com.

CRediT Authorship Contributions

Rui yan, MD (Conceptualization: Equal; Data curation: Equal)
Jianjian Li (Data curation: Equal)
Zeru Xiao (Data curation: Supporting; Methodology: Supporting)
Xiaona Fan (Methodology: Supporting)
Heshu Liu (Formal analysis: Supporting; Methodology: Supporting)
Ying Xu (Formal analysis: Supporting)
Ruya Sun (Writing – original draft: Supporting)
Jian Liu (Writing – review & editing: Supporting)
Jiannan Yao (Formal analysis: Supporting)
Guangyu An (Supervision: Supporting)
Yan Shi (Writing – review & editing: Supporting)
Yang Ge (Conceptualization: Equal; Supervision: Equal)

Conflicts of interest

The authors disclose no conflicts.

Funding

Supported by grant 7202051 from the Natural Science Foundation of Beijing Municipality (Y.G.).